4. 2. Epicenter area determination.

The evolution of seismic prediction was, at its start, initiated, with efforts to determine the time of occurrence of the next strong EQ, which would take place in a seismogenic area. These efforts, intrinsically, incorporated the assumption that, the seismogenic area was known in advance. Therefore, this approach represents the first approximation of the epicentral area determination of a pending, strong EQ. This notion explains the reason, why a lot of efforts were dedicated in the time prediction, at the early stages of the evolution of earthquake prediction.

The next prognostic parameter, that is the location of the future, strong EQ, needed a statistical treatment of the past seismic history of regional areas, in order to reach a conclusion about the probability for the occurrence of a strong EQ in a predefined, seismogenic area. Such types of studies are referred, as "spatial-temporal" studies. In these studies, the spatial distribution of strong EQs and the time of their occurrence are interrelated, so that some well-defined rules are justified, answering both questions "where" and "when" the next strong EQ will take place. Some typical examples, of such studies, were presented by: Wyss and Baer (1981), for the case of Earthquake Hazard of the Hellenic Arc, Keilis-Borok and Rotwain (1990), when they studied the diagnosis of time of increased probability for strong earthquakes in different regions of the world, using the algorithm CN, Romachkova et al. (1998), when they performed intermediate-term predictions in Italy, using the Algorithm M8, Sobolev (2001), when he studied the earthquake preparation in Kamchatka and Japan, using the RTL parameter, Sobolev et al. (2002), when they studied the phases of earthquake's preparation and by chance test of seismic quiescence anomaly in conjunction to the RTL method for the Kamchatka region, Di Giovambattista and Tyupkin (2004), when they studied the seismicity patterns before the M=5.8 2002, in Palermo (Italy), earthquake along to seismic quiescence and accelerating seismicity, Ogata and Zhuang (2006), when they analyzed Space-time ETAS models.

An, entirely, different problem is posed when the seismological data of an area, are very poor or non-existent. It is obvious that in such a case, spatial-temporal methodologies will fail. This was the case of Kozani, Greece EQ (M=6.6, 1995) and Athens, Greece EQ (M=5.9, 1999). Both areas were considered as "safe", in terms of seismic hazard, but Nature proved unpredictable. Therefore, it is evident that, it is necessary a method to exist which will provide, in a way, the epicentral area, independently from the past statistical, seismicity study of the regional area.

In section **(4.1),** was presented the methodology for the determination of the time of occurrence of an earthquake. Next logical question to be asked is: where is this specific earthquake going to take place. Solving this problem, independently from seismic statistics and previous knowledge of seismogenic areas, it requires the activation of a mechanism, which is capable to modify the physical properties of the regional space in a way that the modified physical parameters acquire directional properties. In other words it is possible to measure directional properties of a generated field which will "point towards" the epicentral area of a future EQ.

Mizutani et al. (1976), after having studied electrokinetic's phenomena, associated, with earthquakes, suggested "if we are capable of detecting the electric current induced by the water flow, we can know the direction of the water flow, and consequently predict the epicenter of the earthquake".

Varotsos et al. (1981, 1984b), related the observed, telluric, precursory signals intensity to the epicentral distance of an earthquake from different, registering, monitoring sites. The determination of the epicentral area was utilized by the use of the "Apollonian circles" and the "**1/r**" law, representing the signal intensity, as a function of distance from the seismic epicenter.

In a closer in terms of physics, different approach, Thanassoulas (1991), using as a basis recordings

of the VAN group, proved that it is possible to determine, the epicentral area of a pending strong EQ, much more accurately, by triangulating the calculated, azimuthal directions of the observed, electric earthquake precursory signals at different monitoring sites. The philosophy behind this methodology is that: although, the intensity of the observed, anomalous field depends on the local, geological conditions, the azimuthal direction of its intensity does not change, since it depends mainly on the regional current flow or the static field distribution, in the crust.

Ifantis et al. (1993) used the very same methodology for the determination of the epicenters of two strong EQs in Greece.

Pham et al. (2001) conducted a small-scale, field experiment at CRG, Garchy France. They recorded, signals in various sites originating from leak currents from the building complex. The origin of these currents was successfully determined by analyzing the azimuthal direction of the recorded signal at each monitoring station.

The three last works, which are referred, starting with Thanassoulas (1991) to Pham et al. (2001) clearly, indicate, that the epicentral area of an impending, strong earthquake can be determined, very accurately, by considering azimuthal directions calculation and triangulation of the anomalous, observed, electrical field, instead of any other statistical method used, so far.

An entirely different methodology, for determining the epicentral area of a strong EQ, is based upon ionospheric perturbations, observed, over the epicentral area, a few days before the seismic event takes place, due to ground tectonic, related, physical processes. The oldest related literature which is traced in various publications is the one by Moore (1964) and Davies and Baker (1965) which deals with the strong EQ of Good Friday, in Alaska, in 1964. More recent papers, related, to the topic of epicenter determination by the use of the study of the ionospheric perturbation, were presented by Depueva and Rotanova (2001), Pulinets et al. (2003), Pulinets (2004), Pulinets et al. (2004), Pulinets (2006).

4.2.1. Basic assumptions.

The problem for the determination of the epicentral area of a strong EQ is generalized as follows: is it possible to identify the location of a future strong EQ, in a wide region, of unknown seismic activity in the past, and of no other geological or tectonic information, available?

Although, as a first approach, the answer to this problem appears to be impossible or rather very difficult, it will be shown that, exists a deterministic solution, based on basic, physics principles of electrical, potential fields. The interesting feature of any electrical field is the fact that it exhibits directional properties. In other words, it is possible to calculate the origin of its generating mechanism, by measuring its components at different locations and by inverting them, after having adopted an appropriate, generating, spatial, physical model.

The first and most basic assumption which is used, in the methodology which is going to be presented is , **the crust – lithosphere system, behaves as a homogeneous media,** as far as it concerns its electrical properties for large wavelengths fields, generated in it. This assumption drastically, facilitates the utilization of further mathematical operations which are required for the determination of the epicentral area. A strong objection, which could be raised, immediately, is: “but the crust – lithospheric system is not homogeneous, in terms of present geology and tectonics”. Well, this is true, if short wave lengths of electrical fields are used compared, with lateral, geological – tectonic discontinuities. On the contrary, if large wavelengths of electric field are used, then the effect of geology – tectonics does not exist and the crust – lithospheric system becomes “transparent” for such electrical field wavelengths and, consequently, it behaves as homogeneous media. Moreover, if the basic, adopted, assumption is false, then the results which are obtained, by using a “false” methodology, will be “false”, too. In case the methodology, to be presented, provides “true” results, complying with the location of actually seismic, strong events which have occurred, then it proves that the basic, adopted assumption is valid.

Various different valid, electrical fields – signals generating mechanisms, which have already been referred in the scientific literature, were presented in section **(3)**. Each scientist defends his own seismic, signal generating mechanism by using robust arguments. The real problem, posed by the earthquake prediction requirement, is: which generating mechanism is valid at each seismic event case, so that it could be used, if possible, for epicenter area determination.

Moreover, what is the physical model, which could be used for calculations of this kind? Further more, if more than one, still unknown, physical mechanisms, is, preseismically, triggered, is it possible to "invert" the resulted, combined field, into its "origin" location? It is evident that, as long as the generating mechanisms which are triggered before any strong earthquake, are unknown, the more difficult, not to consider it as impossible, the solution of this problem, is.

A solution for this problem, based on principles of Applied Geophysics, was presented by Thanassoulas (1991). In this case, the geophysical notion of "apparent", physical value was applied to the case of the seismogenic area which generates electrical, preseismic signals, due to various, triggered, physical mechanisms. In particular, **the total, observed, electrical field that results from the combination of the different sub-electrical fields which are generated by the various, triggered, physical mechanisms, is attributed to a single, fictitious, point current source (Apparent Point Current Source). This current source generates, exactly, the very same preseismic, electrical field.**

This is the second assumption upon which the entire methodology is based on. Its validity will be proved by the results which are obtained by applying the methodology on real, preseismic, electrical data.

Schematically, the entire notion of the apparent point current source is presented in the following figure **(4.2.1.1)**.

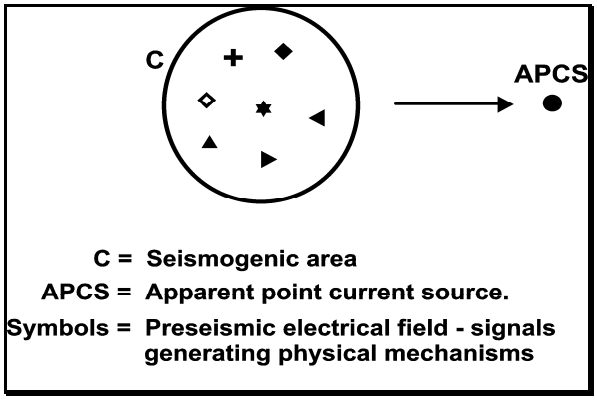

Fig. 4.2.1.1. Various, physical mechanisms (symbols), generating electrical, preseismic signals, triggered, in a seismogenic area **(C),** substituted by a fictitious "apparent" point current source **(APCS)** which generates the very same preseismic electrical signals.

The main advantage of the adoption of the APCS, as it will be demonstrated later on, is the simplification of the mathematical analysis, as far as it concerns the determination of the epicentral area determination of a strong future earthquake.

A generalized, representative model, for the case of generation of a preseismic, electrical field, is presented in the following figure **(4.2.1.2)**.

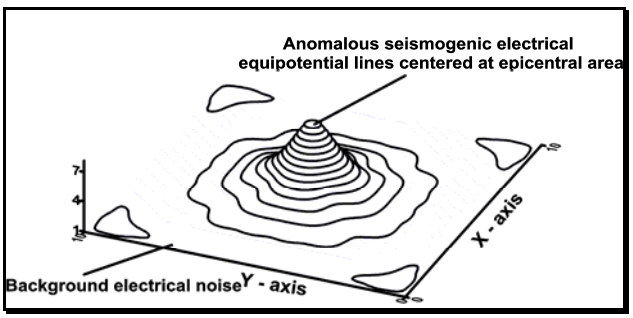

Fig. 4.2.1.2. The preseismic, electrical field, which is generated, by the APCS forms circular, equipotential lines on ground surface, centered, at the epicentral area is presented. The horizontal plane represents, apart from the ground surface, the ambient noise level, present, in the seismogenic area.

The preseismic, electrical signal (field), in most favorable cases, when a strong EQ is pending, exceeds the ambient noise level and is easily detectable. In cases, when the signal (field) amplitude is of lower level than the ambient noise, then it requires specific methodologies in order to be applied, so that the signal to noise ratio is improved at an acceptable and useful level.

This generalized model, of the preseimic, electrical field, which is observed over the focal area, provides a physical explanation for the ionospheric perturbations (electron, plasma densities), which are observed over the epicentral areas, some days prior to the occurrence of strong EQs. The assumed mechanism indicates that the generated, preseismic electrical field penetrates (Horn et al. 2007) the ionospheric layers at heights of almost 100-200Km and therefore, acting as a static, electric field lens, it modifies, circularly, the spatial distribution of the plasma ions, which align along the equipotential surfaces of the preseismic, electrical field which is present, at these heights.

The perturbing mechanism is shown, in a simplified presentation, in the following figure **(4.2.1.3)**.

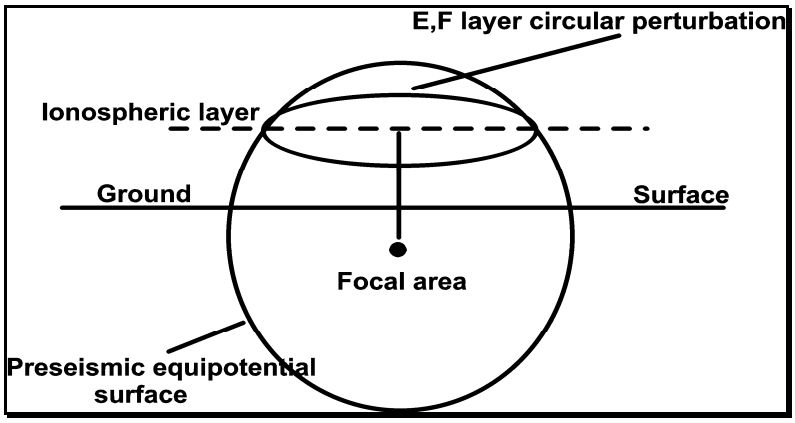

Fig. 4.2.1.3. A simplified model is presented of the perturbing of the ionospheric layers **E, F** mechanism, due to the presence of the preseismic, electric field, which is generated a few days before the occurrence of the pending, strong EQ.

A more detailed presentation of this mechanism is presented in the following figure **(4.2.1.4)**.

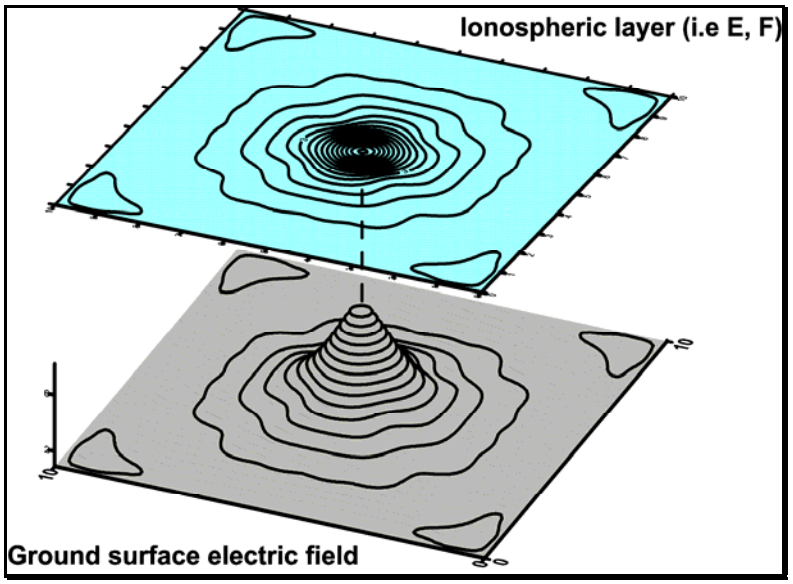

Fig. 4.2.1.4. Plasma – electron density perturbation of the ionospheric layers **E, F** (upper map), due to the presence of a preseismic, electric field on the ground surface (lower map), penetrating the ionospheric layers.

Actually, what happens is that, the concentric, equipotential lines, generated, by the intersection of the **E, F** ionospheric layers with the equipotential surfaces, which surfaces are generated from any triggered, physical mechanism in the focal area, form a local, circular, plane electrical field (its gradient pointing to its center) in the ionosphere, which attracts inwards or repels outwards, charged ions, depending on the polarity of the electrical field. Therefore, in the ionosphere, form circular perturbations of electron – plasma density. This is what is demonstrated in figure **(4.2.1.4)**.

Although, this mechanism seems simple, other electrical fields which are generated in the ionosphere affect the created, preseismic, ionospheric perturbations. Consequently, the ionospheric data, must be demasked from such effects, before any conclusion is made about any suspected, epicenter area of a future strong EQ. Indicative examples, of such operations, have been presented by Depueva and Rotanova (2001).

The previously, presented, physical mechanism validates from another point of view (the one of ionospheric observations), the presence in the seismogenic area of an anomalous, preseismic, electrical field which gives rise to various, preseismic, electrical signals. This electrical field exhibits directional properties and therefore, it is possible to determine its location of origin by applying simple electric, potential theory physics laws.

4.2.2. Preseismic signals amplitude in terms of their period / frequency.

A topic that is important for the study and analysis of the electrical, preseismic signals is their amplitude, as a function of frequency. Generally, it is accepted that, in the phase of preparation of a strong earthquake, strain charge affects the lithospheric – crustal blocks of various sizes. Therefore, the appropriate, electrical, signal is generated, with the corresponding frequency – period, depending upon the size of the strain-charged block. It is understood that small size strain-triggered blocks will generate short wavelengths and consequently, high frequencies, while, large tectonic blocks will generate larger wavelengths and therefore, much lower frequencies.

Furthermore, the energy, which is released by any triggered, tectonic block, depends upon its size. It is evident that tectonic blocks of large volume, will emit larger amounts of energy, in terms of electromagnetic radiation, compared, to small size tectonic blocks, during their fracturing process. The result of this physical mechanism is that, long period, preseismic, electrical signals will exhibit larger amplitudes, compared, to shorter wavelengths. The latter is demonstrated in the following figure **(4.2.2.1)**.

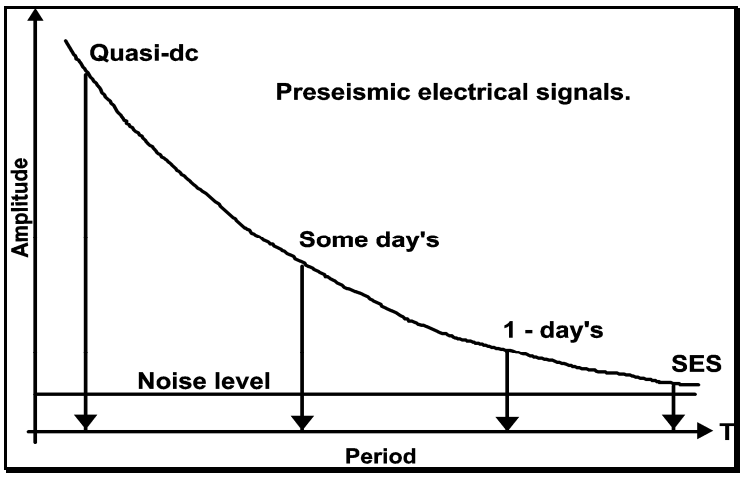

Fig. 4.2.2.1. Preseismic, electrical signal amplitude is presented, as a function of its period.

If a certain noise level, is accepted to be present at the area where the registration of the Earth's electric field takes place, it is evident from figure **(4.2.2.1),** that in terms of noise to signal

ratio, it is advantageous to study the longer wavelengths, instead of the shorter ones, as far as it concerns the preseismic, electrical signal recognition.

By comparing the different period, preseismic, electrical signals to each other, the largest amplitude is met at "**quasi-dc**" signals. This type of signals exhibits such a large period, which can be treated as a "**DC**" current signal. Electrical signals, with a period of a few days exhibit comparably to the "quasi-dc" ones, lower amplitude, and the same is observed for signals with a period of one day.

The case of **SES** preseismic signals, studied by the VAN research team, exhibits the lowest signal to noise ratio, due to their very short period (of a few minutes).

Below, are some representative examples of such type of signals, recorded, by **PYR** monitoring site, before Kythira strong EQ (8th January, 2006, M=6.9). The first two examples (**fig. 4.2.2.2, 4.2.2.3**) are a comparison of the amplitudes of monochromatic (single frequency), preseismic, electrical signals at periods of T=14 and T=1 days.

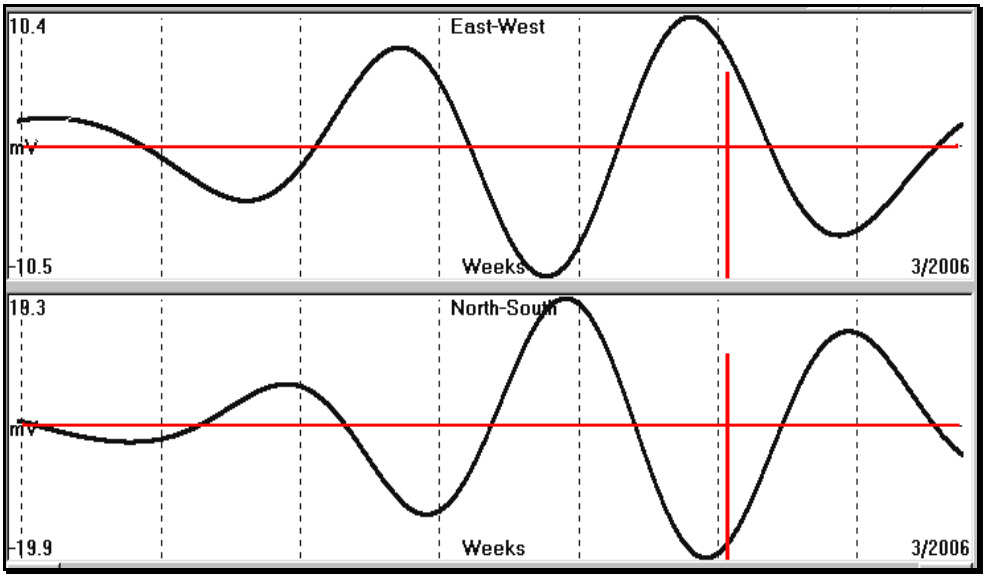

Fig. 4.2.2.2. Oscillatory, preseismic, electrical signal (T = 14 days), observed, by **PYR** monitoring site before Kythira strong EQ (8th January, 2006, M=6.9). The red bar indicates the time of occurrence of Kythira EQ.

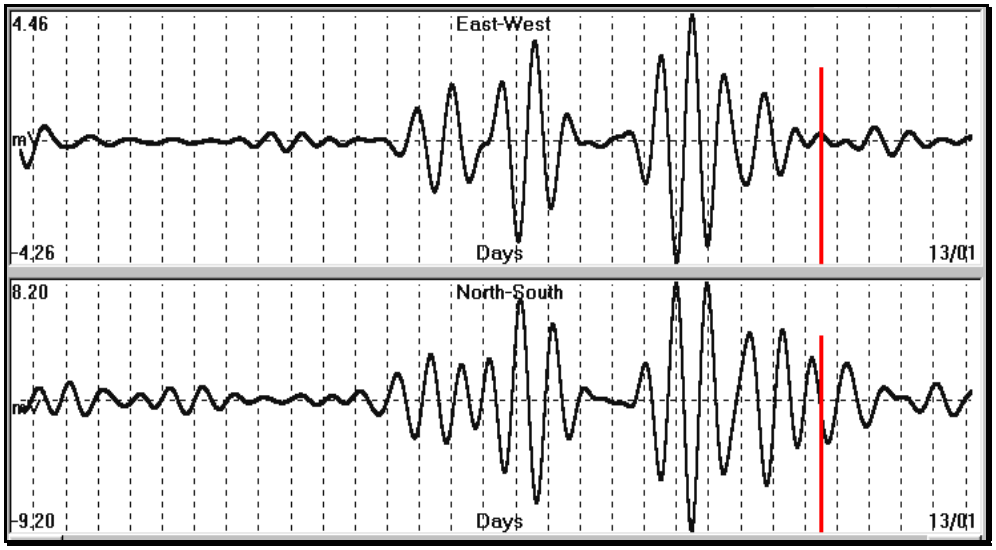

Fig. 4.2.2.3. Oscillatory preseismic electrical signal (T = 1 day), observed, by **PYR** monitoring site before Kythira strong EQ (8th January 2006, M=6.9). The red bar indicates the time of occurrence of Kythira EQ.

The largest period (T = 14 days), preseismic, electric signal has been registered with maximum amplitude of 39.2 mV p-p **(fig. 4.2.2.2),** while in the shorter period (T = 1 day) the corresponding, monochromatic signal exhibits amplitude of only 17.4 mV. A similar decrease in amplitude has been observed in non-oscillatory, preseismic, electrical signals, recorded, by the same **(PYR)** monitoring site which had preceded the same strong EQ (8th January, 2006, M=6.9).

The preseismic, electrical signal, observed, some weeks prior to Kythira EQ, is presented in the following figure **(4.2.2.4)**.

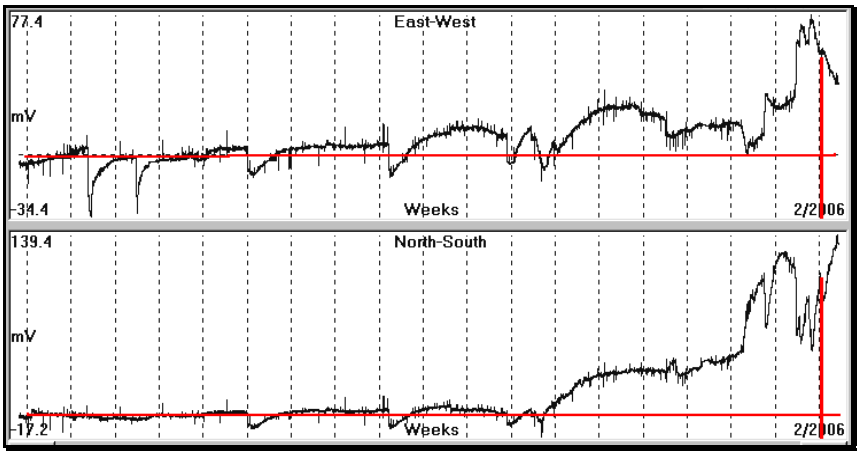

Fig. 4.2.2.4. Preseismic, electrical signal (T =6 weeks), observed by **PYR** monitoring site before Kythira strong EQ (8th January, 2006, M=6.9). The red bar indicates the time of occurrence of Kythira EQ, while the horizontal red line indicates the zero-reference level.

The preseismic, maximum, anomalous signal amplitude, observed, of the Earth's electric field, is of the order of 120 mV (NS component). The case of a shorter wavelength is presented in the following figure **(4.2.2.5)**.

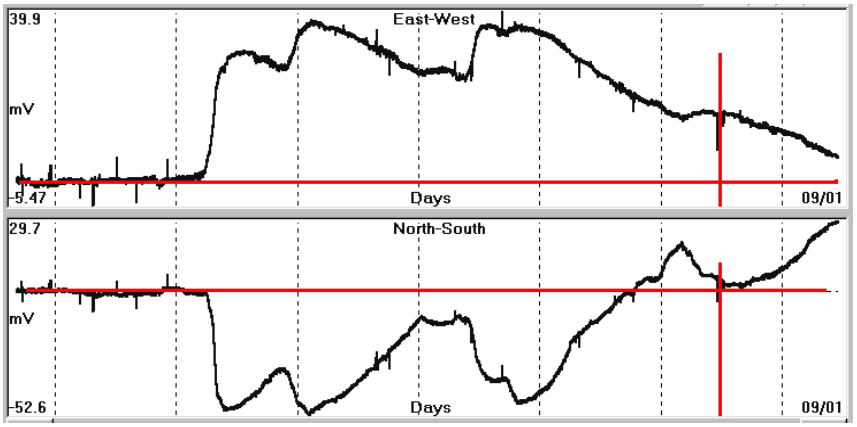

Fig. 4.2.2.5. Preseismic, electrical signal (T = 4 days), observed, by **PYR** monitoring site before Kythira strong EQ (8th January 2006, M=6.9). The red bar indicates the time of occurrence of Kythira EQ, while the horizontal red line indicates the zero-reference level.

In this case, a period of T = 4 days is presented in the graph. The maximum amplitude, observed, in this case, is –52.6 mV which is less than half the amplitude of the previous case. The main conclusion from this presentation is that, preseismic, electric signals, of very long period, exhibit larger amplitudes and therefore, are more easily detectable, due to their high signal to noise ratio. Consequently, these signals are more useful for any further processing procedures, aiming into calculating the prognostic parameters of a pending strong EQ.

4.2.3. What is actually measured.

So far, it has been made clear, concerning the preseismic electrical signals, that various generating physical mechanisms do exist and that the generated signal amplitude depends upon its wavelength (period / frequency). These preseismic, electric signals are received by appropriate electrode arrays, which are used for their registration. The question which arises immediately, is: which physical quantity is measured on the ground surface by using any electrical array (dipole)? This question will be answered in detail as follows.

Let us assume that a seismogenic area has been activated and generates, by any acceptable and valid physical mechanism, a potential **(P)** at its focal area. The potential **(P1),** exactly above its focal area, at the epicenter, will exhibit slightly lower amplitude than **(P),** due to the fact that the epicenter is located at some distance **(x),** far from the focal area and moreover the potential **(Pr),** at any distance **(r)** from its origin, it will be a function of distance **(r)** and the time of observation **(t)**.

$$Pr = f(r,t) \qquad (4.2.3.1)$$

Adopting the **point current source,** as the generating mechanism, the potential **(Pr),** as a function of distance from the epicentral area, is shown in the following figure **(4.2.3.1)**.

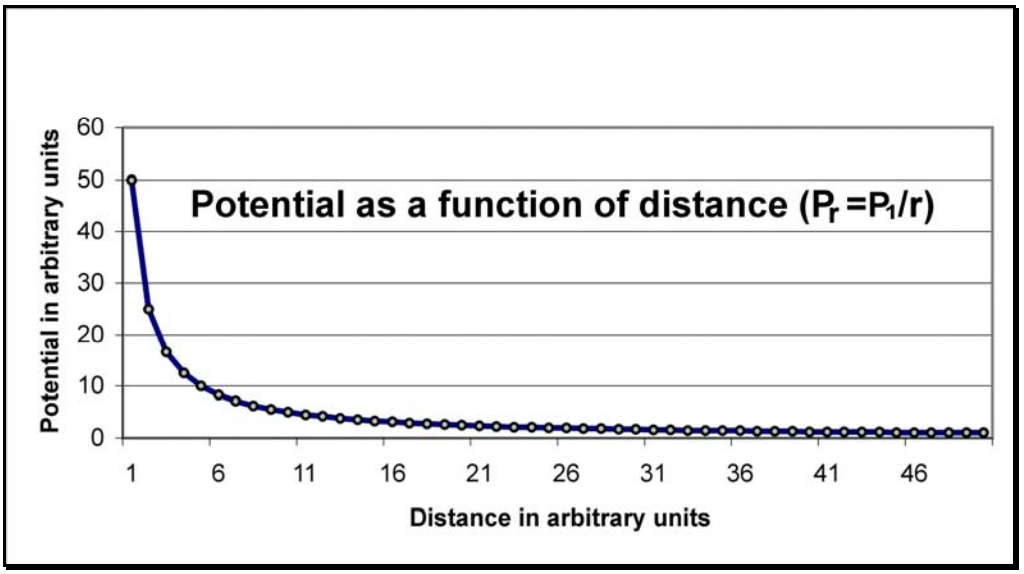

Fig. 4.2.3.1. Schematic presentation of the potential **(Pr)** at a location, as a function of its distance **(r)** from the epicenter area of a pending, strong earthquake, is shown.

The registration of the Earth's potential is made through the use of a pair of electrodes, forming a dipole of length **(x)** in contact to the ground. Therefore, what is actually measured is the potential field quantity:

$$dP = \partial P/dxdt \qquad (4.2.3.2)$$

assuming that:

$$dx \blacktriangleright dr \qquad (4.2.3.3)$$

then equation **(4.2.3.2)** can be written as:

$$dP = \partial P/drdt \qquad (4.2.3.4)$$

that is the time / distance gradient of the potential field which is generated in the focal area.

This is demonstrated in the following figure **(4.2.3.2),** where a pictorial view indicates the quantity, measured, by the used dipole.

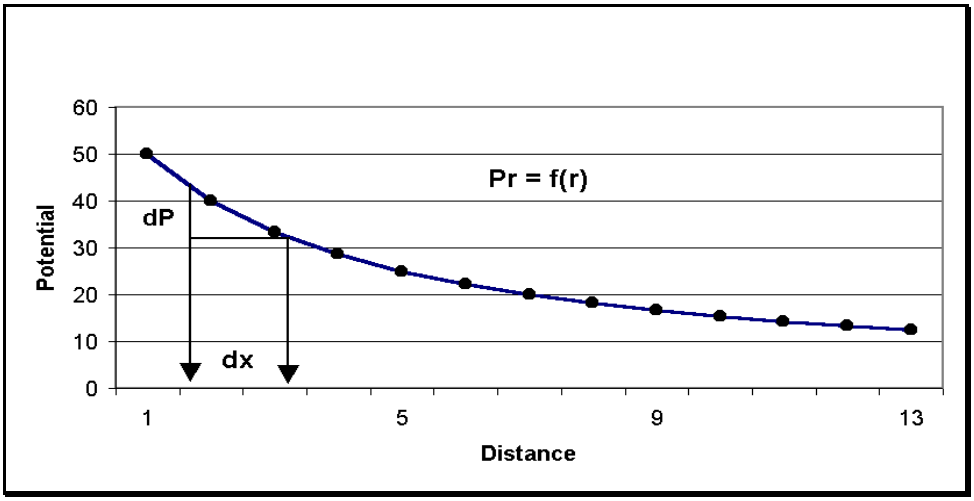

Fig. 4.2.3.2. Graphic representation of the quantity **(dP),** measured, by a pair of electrodes, which are inserted in the ground at distance **(x)** between each other.

The true form of the generated potential, as a time-function, is obtained after integrating the equation **(4.2.3.4)** in time**.** At this point, let us recall, the stress-strain relation (left) of a stress charged, deforming solid and the corresponding potential-time (right) curve, which is generated when the stressed material exhibits piezoelectric properties, presented in the following figure **(4.2.3.3)**.

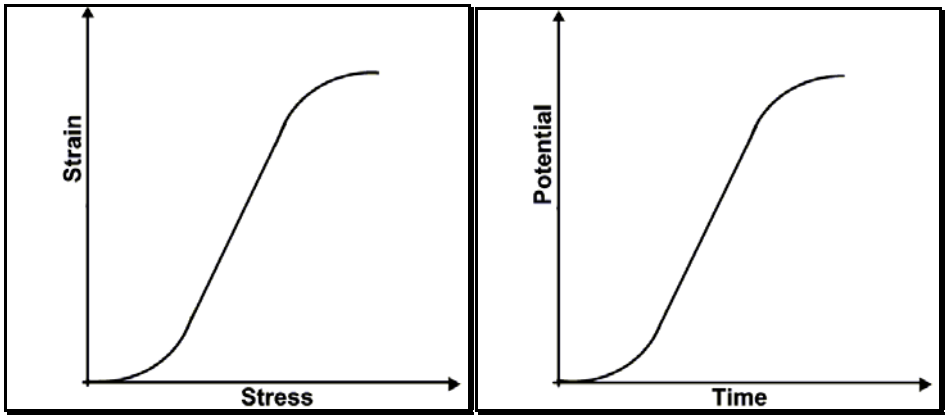

Fig. 4.2.3.3. Typical stress – strain relation of solid material and its corresponding, potential – time relation which exhibits any, stressed material that exhibits piezoelectric properties.

The figure on the right represents the total potential which is generated by the piezoelectric mechanism. The registered on ground surface, potential gradient which is generated by any activated, physical mechanism in the focal area, after its integration in time, will present its original, potential form. Consequently, if the resulted potential, after this operation (integration) presents the form of the right part of figure **(4.2.3.3),** then it is justified to accept that the main, generating mechanism is the piezoelectric one, activated in the crust, due to the presence of the quartzite and stress increase.

The issue of the piezoelectric mechanism has been objected strongly by many researchers.

The main objection is that, quartzite crystals are randomly, oriented, in space and therefore, the potentials which are generated by single crystals are cancelled out by others, of opposite polarity, in the crust. This leads to a neutral, electrical property of the crust. This point of view is strongly debated by the fact that, during crystallization, various factors affect the orientation of the crystals main axis.

Probably, the main factor is the stress, present in the media of crystallization. Another one is gravity and weight load charge, due to overlaying, geological formations. Large tectonic movements, also, change the crystal axis orientation of the quartzite crystals, which are contained in large, geological blocks. Moreover, even if it is accepted that there is a smooth, random orientation of the quartzite crystals, still only the crystals which have their main symmetry axis, aligned, to the stress orientation will generate piezoelectric potential. In this case, it is very difficult to adopt the idea that there is a "perfect" match, of the opposite polarity of the activated crystals, which cancels out the generated potential. This is especially more difficult, if the fact that the crust is not a perfect, homogeneous, electrical medium, is taken into account. Furthermore, the piezoelectric properties of the quartzite are so large, compared to other materials, that even a small amount of deviation of "perfect, main symmetry axis orientation" cancellation will produce potentials, observable, on ground surface at large distances. The reason which justifies the use of quartzite in various applications by the industry, from crystal oscillators in radio transmitters to small lighters, is exactly its large piezoelectric property, compared to any other.

Another objection, arising, against piezoelectricity is that, the generated potentials fade out quickly, because of Earth's high conductivity. The work of Blohm (1977), who suggests a highly resistant crust (100000 Ohmm), at the main, seismogenic zone, when we refer to the conductivity of the Earth, must be recalled. The presence of the piezoelectric, generating mechanisms, which are activated in the focal area, in a highly resistant medium, facilitates the generated potentials to be sustained furthermore and to propagate at long distances with no appreciable attenuation. Therefore, the argument of the conductive Earth does not apply in the seismogenic zone of the crust.

Apart from these, "for and against" arguments, piezoelectricity is the only, known mechanism, which justifies the generation of long period oscillating signals (T = 1, 14 days), due to the fact that it responds to the (induced by the tidal waves) strain deformation of the, subjected, in stress, material, as long as the stress lasts.

The validity of the piezoelectric mechanism will be proved by two examples of strong EQs which were preceded by electrical signals of the piezoelectric mode **(fig. 4.2.3.4)**.

The first example is the one of Izmit, EQ (M = 7.8, 17th August, 1999) in Turkey**.** The preseismic, electrical signals were recorded at a distance of 650Km from Izmit, in Volos **(VOL)**, Greece, with a dipole of 120m, oriented, NS.

The registered, raw data are presented in figure **(4.2.3.4)**.

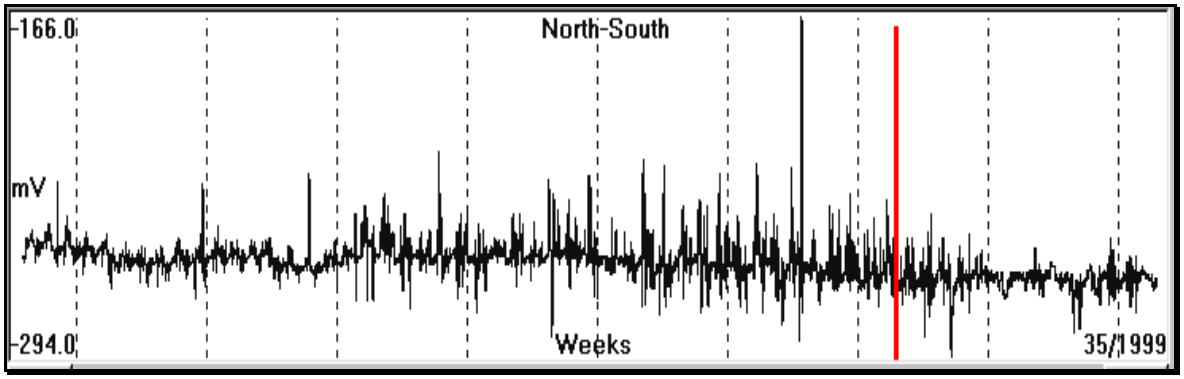

Fig. 4.2.3.4 The Earth's electric field, as it was recorded in Volos **(VOL)**, Greece for a two months period (1st July – 30th August 1999). The red bar indicates the time of occurrence of Izmit EQ (M = 7.8, 17th August 1999).

The recorded signal indicates some “noise” increase for some days before the occurrence of the EQ. Regardless the nature of this “noise”, the raw signal must be detrented, so that the superposed DC component, is eliminated. This operation is presented in the following figure **(4.2.3.5)**.

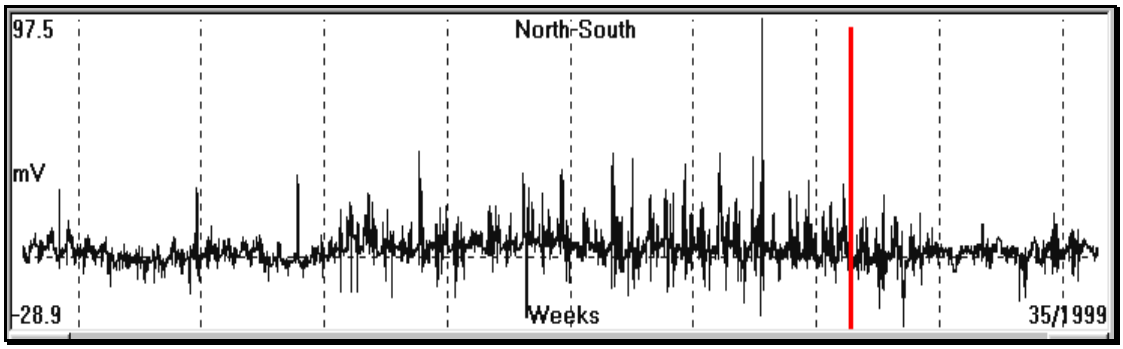

Fig. 4.2.3.5. Detrended raw data of figure (4.2.3.4). The red bar indicates the time of occurrence of Izmit EQ (M = 7.8, 17th August 1999).

Finally, integration is performed along the detrended data and the original potential, which was generated by the physical mechanism, and was triggered in the focal area, has the form of the figure **(4.2.3.6)**.

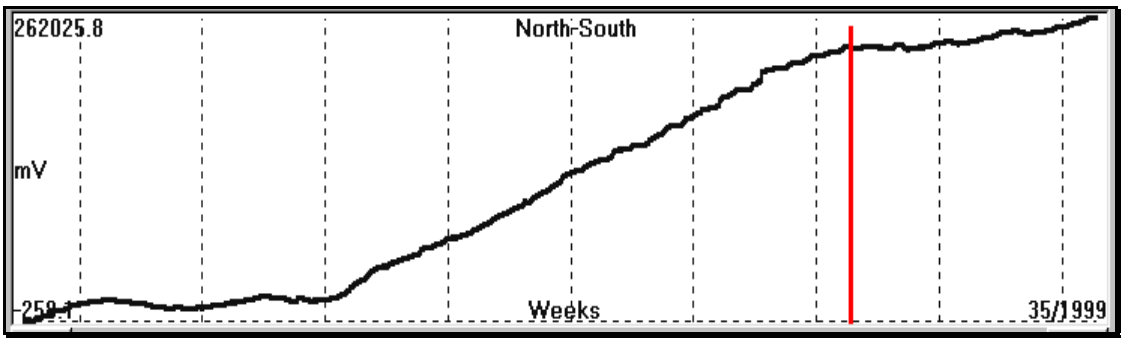

Fig. 4.2.3.6. Form of the potential, generated, by the physical mechanism, triggered, in the focal area of Izmit EQ (M = 7.8, 17th August, 1999).

Next figure **(4.2.3.7)** compares the potential results, which are obtained, from the processing of the Izmit, registered, data to the theoretical ones, which are indicated, by the adopted, piezoelectric mechanism.

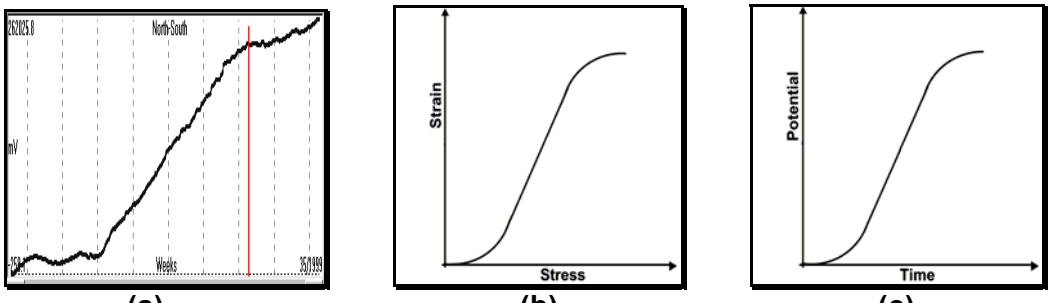

(a) **(b)** **(c)**

Fig. 4.2.3.7. Potential generated by the piezoelectric mechanism **(a),** compared with the theoretical, piezoelectric model **(c)** and the triggering stress, inducing mechanism **(b).**

It is worth to notice that the earthquake occurred, as it was predicted by the stress-strain curve following the rock-mechanics fracturing laws.

Next example is the one of Milos, Greece EQ (M = 5.6, 21st May, 2002). The raw data which were recorded for a period of two months (31st December 2001 – 1st June 2002) are shown in the following figure **(4.2.3.8)**.

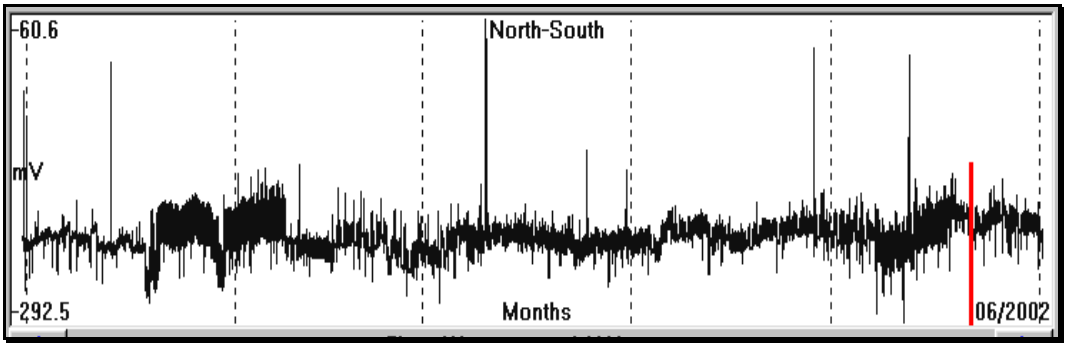

Fig. 4.2.3.8. The Earth's electric field as it was recorded in Volos **(VOL)**, Greece for a two months period (31st December, 2001 – 1st June, 2002). The red bar indicates the time of occurrence of Milos EQ (M =5.6, 21st May 2002).

The recorded signal indicates some "noise" increase for some days before the occurrence of the EQ and a similar one 3.5 months before. The same, detrending operation was applied in these data, too, so that the superimposed DC component is eliminated. This operation is shown in figure **(4.2.3.9)**.

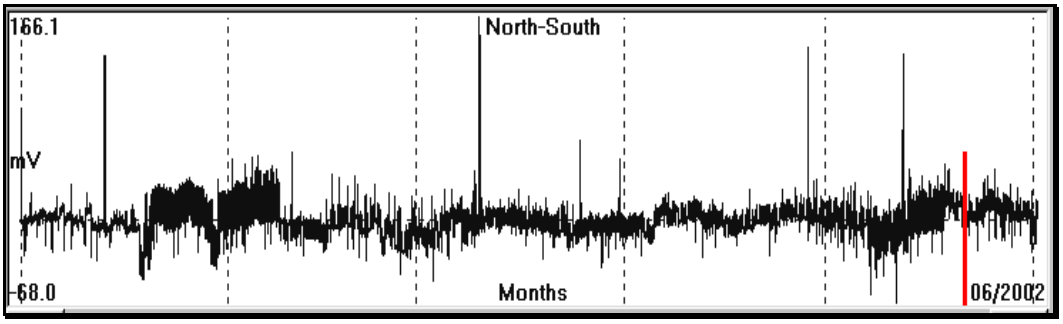

Fig. 4.2.3.9. Detrended data of Milos EQ. The red bar indicates the time when this earthquake occurred (M =5.6, 21st May 2002).

Finally, integration is performed along the detrended data and the generated, original potential, by the triggered, physical mechanism, in the focal area, has the form of the figure **(4.2.3.10)**.

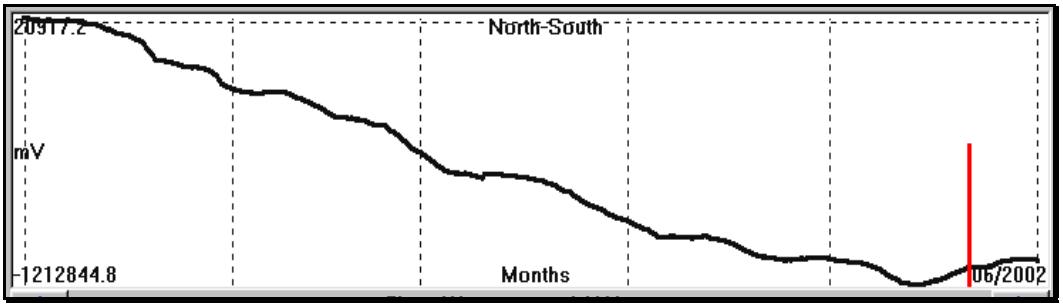

Fig. 4.2.3.10. Form of potential, generated, by the physical mechanism, triggered, in the focal area of Milos EQ (M =5.6, 21st May, 2002).

Next figure **(4.2.3.11**) compares the potential results which are obtained, from the processing of Milos EQ, registered, data to the theoretical ones, indicated, by the adopted, piezoelectric mechanism.

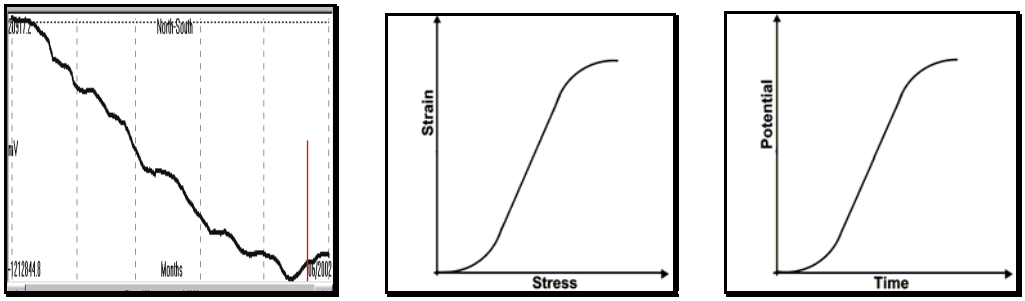

(a) **(b)** **(c)**

Fig. 4.2.3.11. Potential generated by the piezoelectric mechanism **(a),** compared, to the theoretical, piezoelectric model **(c)** and the triggering stress, inducing mechanism **(b).**

The decrease of potential, observed, in **(a)** is due to the fact that, negative polarity potential is generated in the focal area. The typical form of figure **(c)** is based on the assumption that positive polarity potential is generated.

Actually, the polarity of the electrical field, generated, in the focal area, depends on parameters still unknown, which must be studied in detail in the future. Nevertheless, the knowledge of the polarity of the generated field is not important, as far as it concerns the methodology which will be demonstrated for the epicenter area determination. The reason will be explained later on, when the details of the epicentral area determination will be presented.

4.2.4. Preseismic signals normalization.

The homogeneous ground Earth model which is adopted in section **2.5.3** implies that a point, current source, located in it, generates equipotential lines on the ground surface. In case of a seismogenic area, where a strong earthquake will take place some time in the close future, the center of the generated, equipotential lines, by the apparent point current source, coincides with the epicenter of the pending earthquake. Schematically it is shown in the following figure **(4.2.4.1)**.

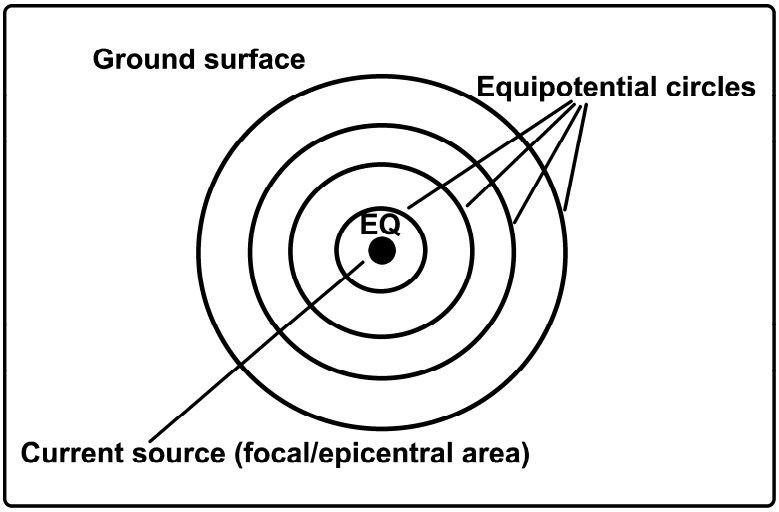

Fig. 4.2.4.1. Schematic presentation of the equipotential lines which are generated on ground surface by the apparent point, current source. This source is located in the focal area, which is centered at the epicentral area of the pending, strong earthquake.

At this stage, it is a simple task to calculate the azimuthal direction of the Earth's electric field intensity vector. The azimuthal direction of the electrical field intensity vector indicates the direction of the location of the apparent point current source, in relation to the registration site. Schematically, this procedure is presented in the following figure **(4.2.4.2)**.

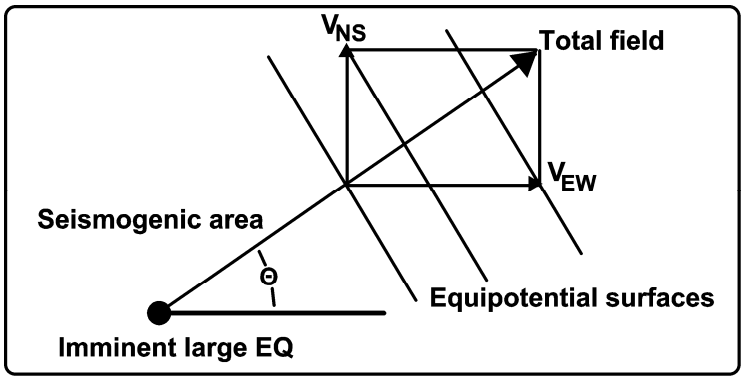

Fig. 4.2.4.2. Azimuthal direction **(θ)** of the Earth's electric field intensity vector calculation related to the location of the registration site.

The actual procedure is as follows:

The Earth's electric field is measured in two orthogonal components V_{NS} and V_{EW}. The next step is to calculate the angle **(θ).** This is achieved through the following trigonometric equation:

$$(\theta) = \arctan (V_{NS} / V_{EW}) \qquad (4.2.4.1)$$

The equation **(4.2.4.1)** is valid assuming that, the registering system complies with the requirements of being a unit trigonometric circle. In other words, the electric dipoles which are used for the registration of the Earth's electric field, must be of the same length and moreover these must be oriented towards **N-S** and **E-W** directions, so that is achieved a geographical orientation of the Earth's electric field intensity vector. The registering dipole system must be equal to the trigonometric circle, shown in the following figure **(4.2.4.3)**.

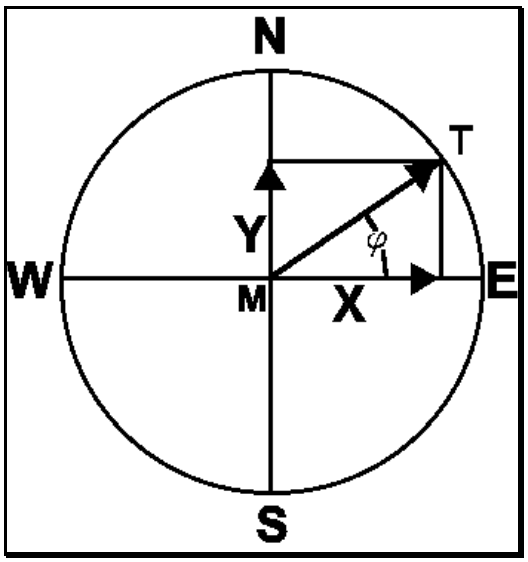

Fig. 4.2.4.3. The trigonometric unit circle is presented, which must reflect the registering system of the Earth's electric field, so that may be achieved an azimuthal determination of the direction of the electrical field intensity vector.

The dipoles, which are used for the registration of the Earth's electric field **(T) X** and **Y** components, must be oriented towards **E-W** and **N-S**. In practice, when a dipole system is to be located at a specific place, the most common situation, met, is that it is not possible to orient the dipoles exactly at **E-W** and **N-S** direction, but at more or less different angles.

Furthermore, it is not easy to lay down electrical lines of the same length, because of local obstacles. These conditions are presented in the following figure **(4.2.4.4)**.

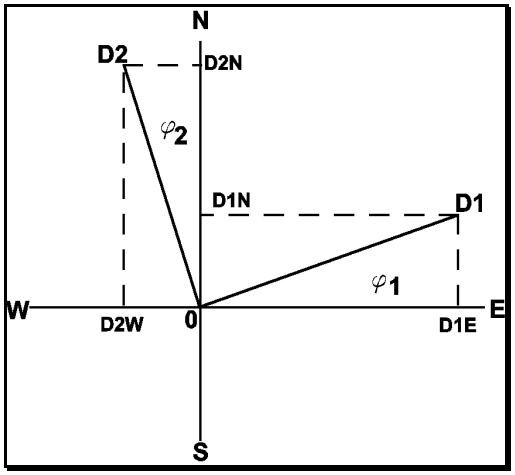

Fig. 4.2.4.4. Schematic presentation of an actual dipole array **(E-W, N-S)** located at ground. The dipole lengths are **O-D2 (N-S), 0-D1 (E-W).** The deviation from real **N-S** direction is **φ2,** while from the **E-W** direction is **φ1**.

The necessity, which immediately arises under such a situation is, obviously, to convert the actual "**field dipole**", into its equivalent trigonometric "**unit circle**". This is performed as follows:

The dipole of length **D1** is decomposed into its two length components, along the **E-W** and **N-S** directions as follows:

$$D_{1E} = D_1 \cos(\varphi 1) \qquad (4.2.4.2)$$

$$D_{1N} = D_1 \sin(\varphi 1) \qquad (4.2.4.3)$$

In the same way the dipole of length D_2 is decomposed into its two length components, along the **E-W** and **N-S** directions as follows:

$$D_{2W} = D_2 \sin(\varphi 2) \qquad (4.2.4.4)$$

$$D_{2N} = D_2 \cos(\varphi 2) \qquad (4.2.4.5)$$

Consequently, the actual dipole length along the **E-W** and **N-S** directions is:

$$\text{E-W dipole length (EW)} = D_{1E} + D_{2W} \qquad (4.2.4.6)$$

$$\text{N-S dipole length (NS)} = D_{1N} + D_{2N} \qquad (4.2.4.7)$$

The final step, towards a trigonometric unit circle conversion of the field dipole array, is to normalize the **(EW)** and **NS** dipole lengths to a unit length. This can be achieved by normalizing the length of one of the two dipoles, no matter which one, to the length of the other. This is, simply, performed by multiplying the length of one (i.e. EW) dipole by the inverse ratio of them (**NS/EW**):

$$EW = EW\ (NS/EW) \qquad (4.2.4.8)$$

The very same analysis holds for the potentials, which are registered from the actual field dipoles. If the "dipole length" is substituted by measured "potential", then the same equations **(4.2.4.2)** to **(4.2.4.7)** hold for the registered potential, too. Finally, the potential which corresponds to the unit trigonometric circle is obtained by the normalization of the **EW** or **NS** potentials to the **EW** or **NS** dipole lengths **by the use of the dipole length ratio NS / EW or EW / NS,** which depends on which direction must be normalized to the other one. The entire procedure is easily programmed in any programming language. Therefore, a number of monitoring sites which use different dipole

lengths and orientations can be, processed, in a very short time, resulting into orthogonal “unit circle trigonometric”, potential measurements, thus, facilitating the azimuthal direction calculation of the Earth’s electric field intensity vector at each monitoring site.

An example of the already presented procedure for the registered Earth’s electric field normalization is presented in the following figures **(4.2.4.5 – 4.2.28)**. The first diagram **(4.2.4.5)** represents the registered Earth’s potential of dipole **(A)** of length **(LA)** and is oriented to an azimuthal direction **(φA)** from the geographical Easting direction.

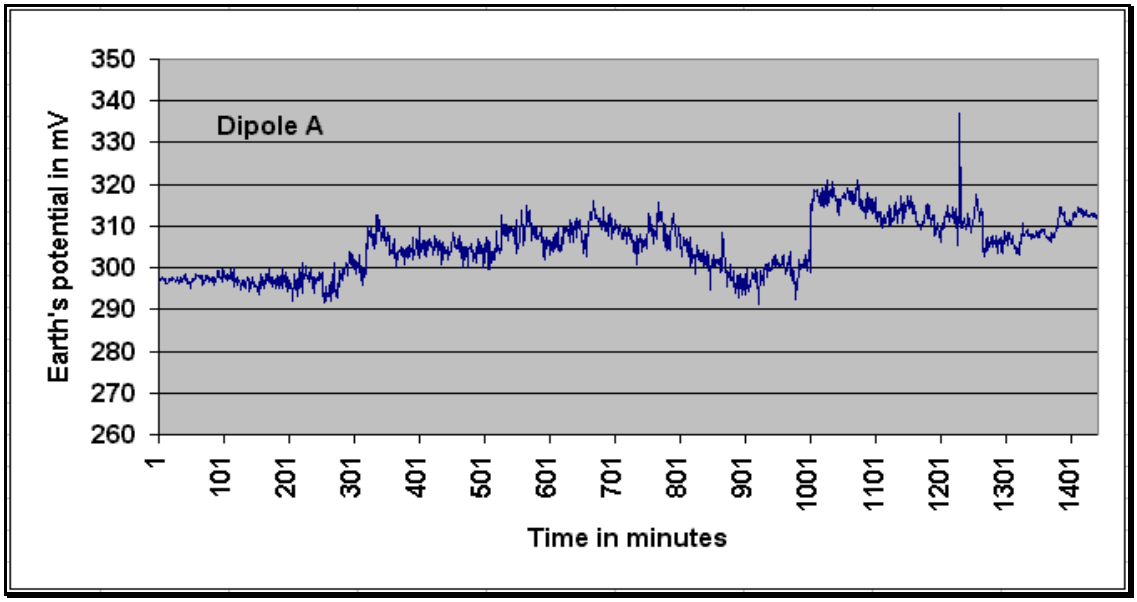

Fig. 4.2.4.5. Presentation of Earth’s electric potential, registered from dipole **(A).**

Next figure **(4.2.4.6)** represents the registered Earth’s potential of dipole **(B)** of length **(LB)** and is oriented to an azimuthal direction **(φB)** from the geographical Northing direction.

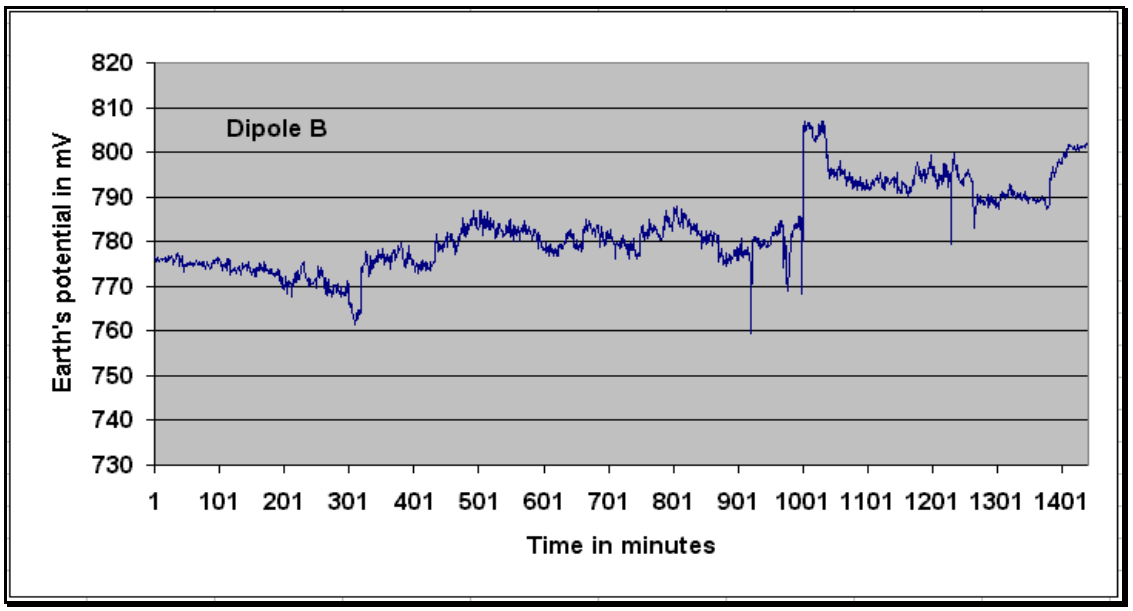

Fig. 4.2.4.6. Presentation of Earth’s electric potential, registered from dipole **(B).**

The procedure of normalization, which is applied to the registration of these two **(A, B)** dipoles, is presented in the following two graphs.

The first graph **(4.2.4.7)** shows the normalized **E - W** dipole registration which results.

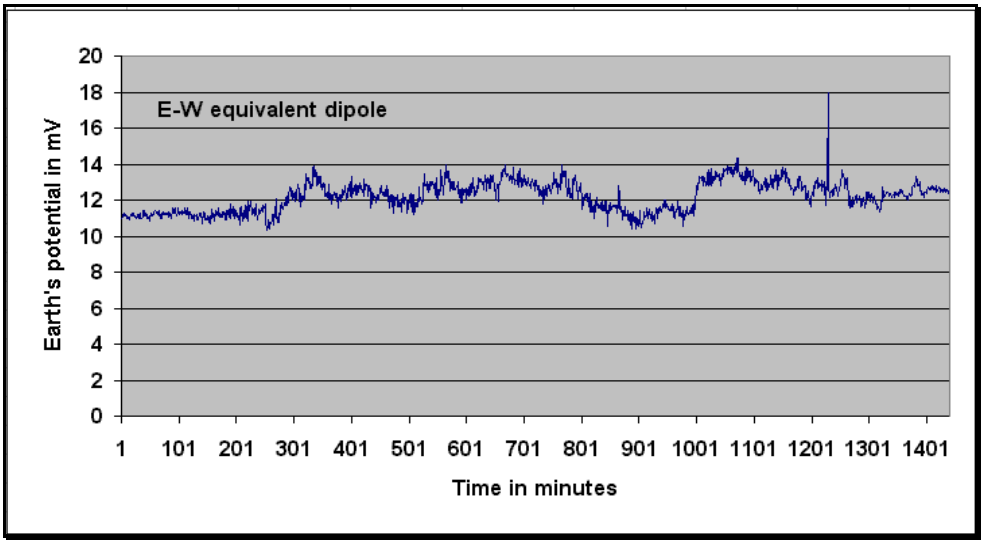

Fig. 4.2.4.7. Presentation of normalized **E – W** Earth's electric, potential field registration.

The second graph **(4.2.4.8)** shows the normalized **N – S** dipole registration which results.

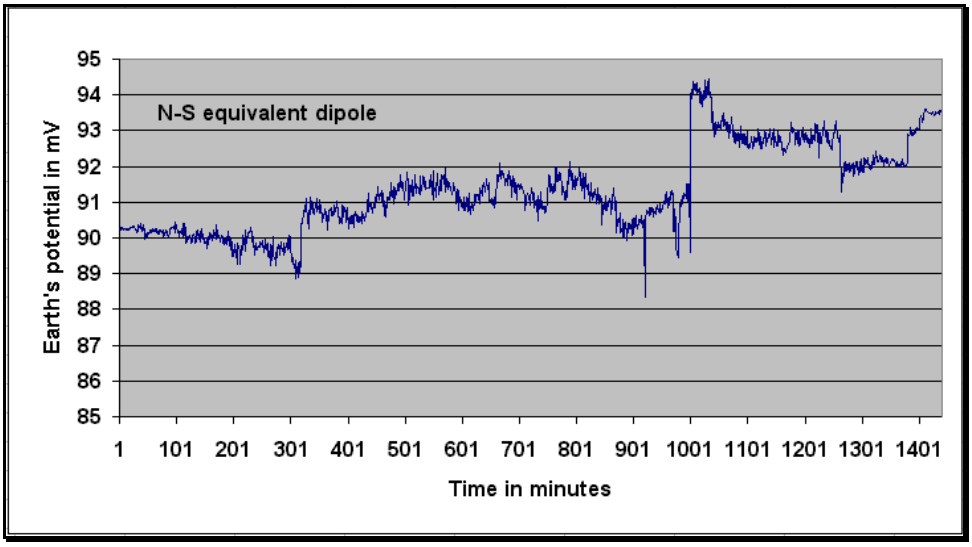

Fig. 4.2.4.8. Presentation of normalized **N – S** Earth's electric, potential field registration.

It is worth to notice the difference, which is observed in the registration levels, between **raw (fig. 4.2.4.5-6)** and **normalized (fig. 4.2.4.7- 8)** electric potential values. This will be analyzed in detail in the section which describes the hardware system, and was constructed for the utilization of this type of registration. The example, which is presented in the figures **(4.2.4.5 - 4.2.4.8)** was recorded by Athens monitoring site, on 27th March, 2007. Below are presented some more examples of normalized registrations, which span over larger time periods and are recorded at the same monitoring site, so that the reader may obtain a full picture of the entire registration procedure.

Figures **(4.2.4.9 – 4.2.4.14)** which follow, represent the Earth's electric, potential, registered for seven (7) days, thirty (30) days, six (6) months, one (1) year, two (2) years and the total registration right from the start of the operation (15th April 2003) of Athens **(ATH)** monitoring site, till 27th March 2007.

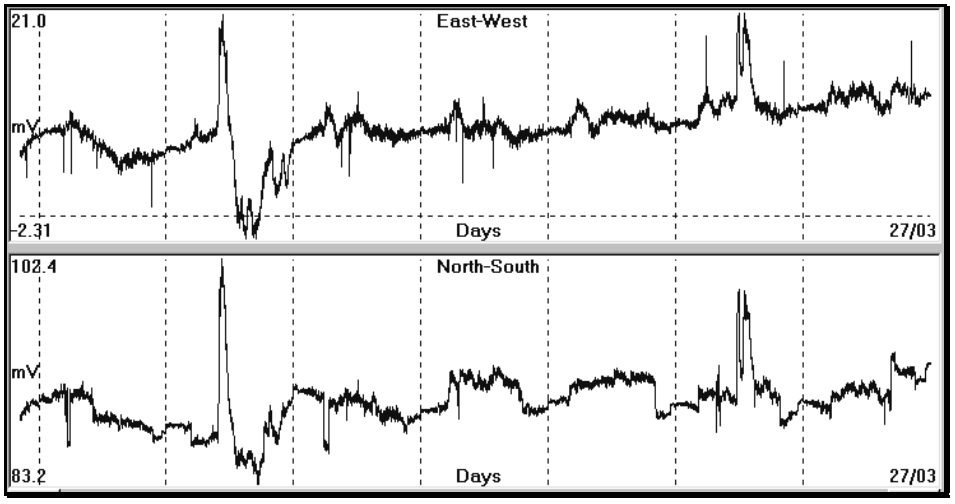

Fig. 4.2.4.9. Presentation of the normalized, registered, Earth's electric field for seven days period from 20th March to 27th March, 2007 by Athens **(ATH)** monitoring site.

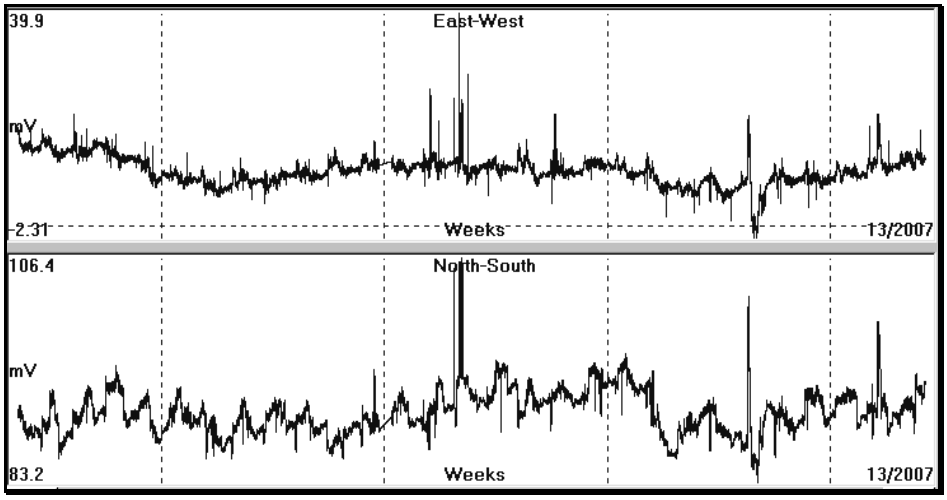

Fig.4.2.4.10. Presentation of the normalized, registered, Earth's electric field for thirty days period from 27th February to 27th March, 2007 by Athens **(ATH)** monitoring site.

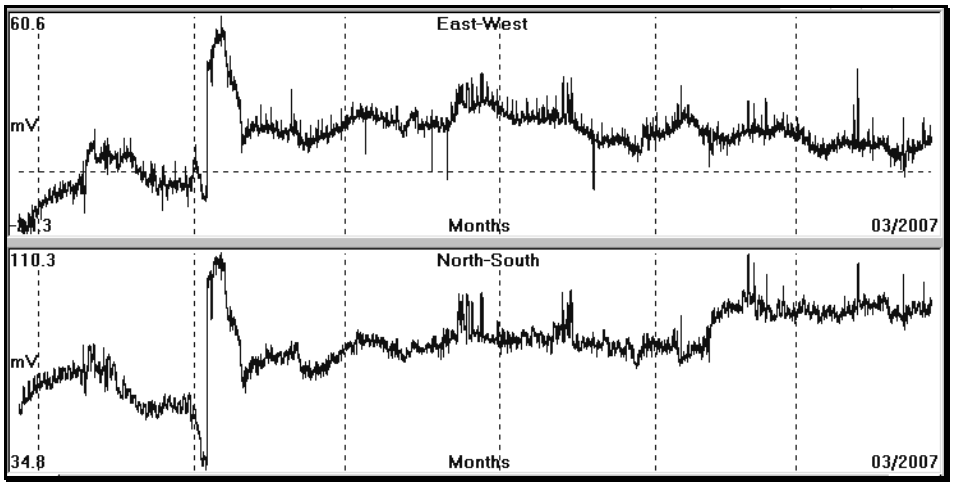

Fig. 4.2.4.11. Presentation of the normalized, registered, Earth's electric field for six months period from 27th September, 2006 to 27th March, 2007 by Athens **(ATH)** monitoring site.

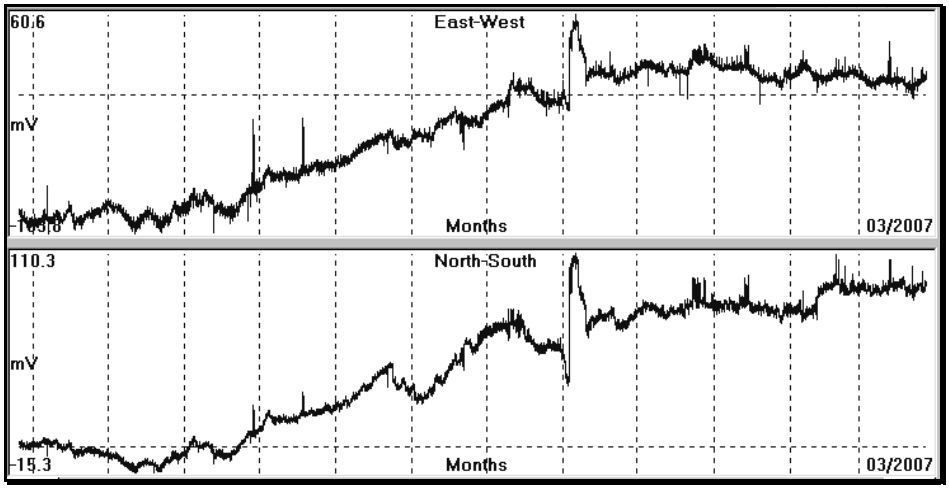

Fig. 4.2.4.12. Presentation of the normalized, registered, Earth's electric field for one year period from 27th March 2006 to 27th March, 2007 by Athens **(ATH)** monitoring site.

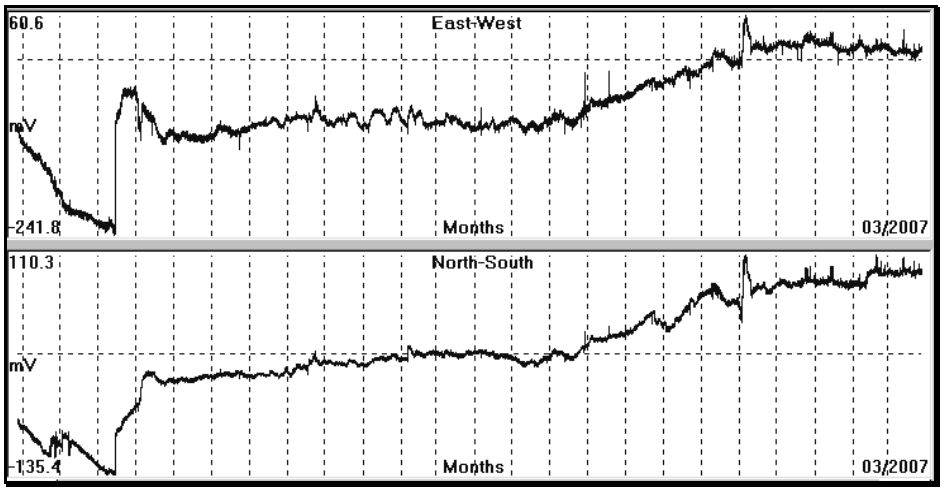

Fig. 4.2.4.13. Presentation of the normalized, registered, Earth's electric field for two years period from 27th March, 2005 to 27th March, 2007 by Athens **(ATH)** monitoring site.

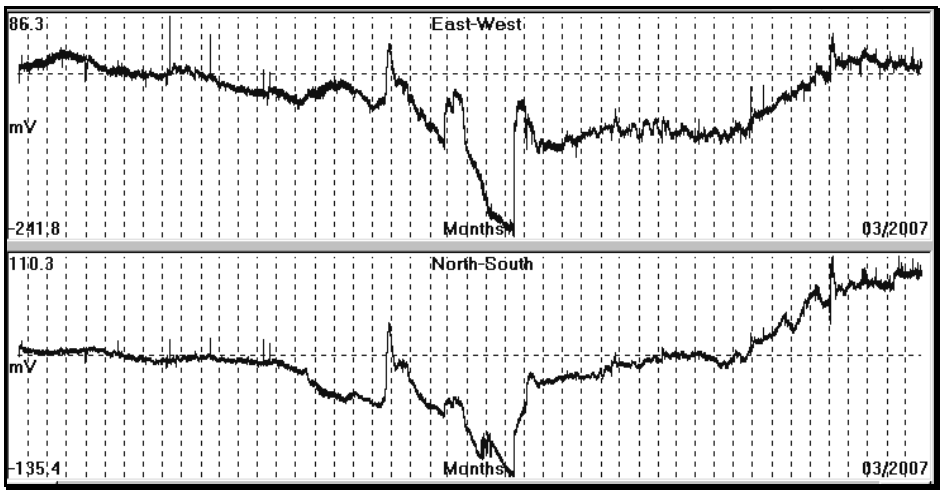

Fig. 4.2.4.14. Presentation of the normalized, registered, Earth's electric field for the total period of recording from 15th April, 2003 to 27th March 2007 by Athens **(ATH)** monitoring site.

At this stage of the analysis which has already been presented, registrations, which comply with the unit trigonometric circle (registered at **N – W, S – E** direction and of equal (unit) dipole length, are available for any further processing. It is anticipated that, at the present time, the Earth's electric field has been contaminated by any type of noise, i.e. anthropogenic, ionospheric, hardware malfunctioning, failure of field installation and practically of any type, you name it.

Consequently, the next stage that follows is the actual editing - filtering techniques, which are required to extract the "real seismic electric" precursory signal, which will be used for the determination of the epicentral area of the imminent large earthquake.

4.2.5. Preseismic, electric signal processing.

Before any use of the data series which result from the acquisition and registration of the Earth's electric field, by any monitoring site, is made, two important operations are applied on them. The first is the editing of the data and the second one is the noise filtering. Details are presented as follows.

4.2.5.1. Data file editing for missing data.

The filtering techniques and methodologies, which deal with time series of any data type, require, as input data, files which are free from data gaps. If, accidentally, a "gap" is met during the processing of a data file, then in most cases, the running procedure, either "crashes" or generates erroneous results. In both cases, it takes some time to be wasted, in order to rectify this nasty situation. Therefore, as a preliminary step, before any methodology is applied on a specific data set, it is a good policy to check against data gaps and to apply any suitable methodology to recover the data continuity.

In the particular case of the registration of the Earth's electric field at the various monitoring sites which are in operation to date **(ATH, PYR, HIO),** the following causes have created data gaps:

a. Damage on the dipole electrode lines. This is mostly a breakdown of the wire which connects the electrode with the preprocessing unit, located, at the housing of the monitoring site.

b. "Crashing" of the computer system, used, due to power line voltage rapid and large amplitude changes, which the used UPS, cannot accommodate.

In both cases, the result is the same. Data gaps are created, since the casual monitoring site operator becomes aware of the faulty situation, only after a few hours from its occurrence.

As long as such a gap has been detected, the gap is replaced by linearly, interpolated data, taking into account the start and the end data values, which preceded and followed the data gap. This procedure is presented in the following figures **(4.2.5.1.1 – 4.2.5.1.3)** which present data gaps, met, at recordings by **PYR** monitoring site.

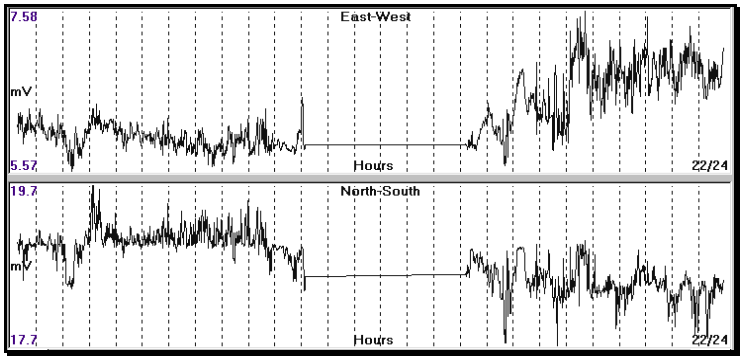

Fig. 4.2.5.1.1. Presentation of "missing data" and their linearly, interpolated values, used to bridge the corresponding data gap. Date of gap recording, 14th November 2006, at Pyrgos **(PYR)** monitoring site.

The observed data gap of figure **(4.2.5.1.1)** lasted for six (6) hours during the actual recording of 14th November, 2006 at Pyrgos **(PYR)** monitoring site. A much longer data gap is presented in the following figure **(4.2.5.1.2)**.

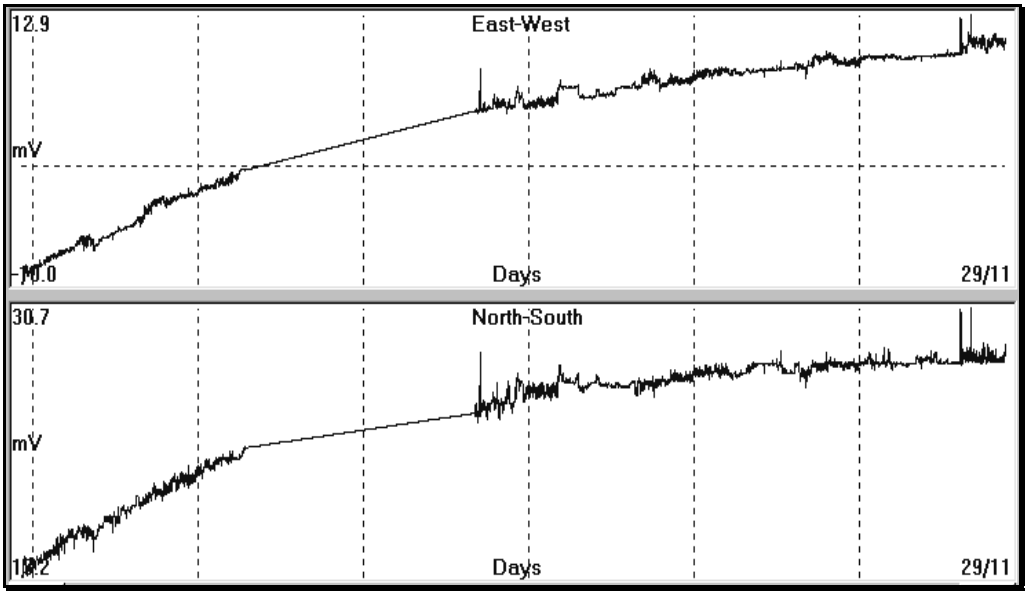

Fig. 4.2.5.1.2. "Missing data" and their linearly interpolated values are presented, which are used to bridge the corresponding data gap. Date of gap recording, 25th-26th November 2006, at Pyrgos **(PYR)** monitoring site.

The observed data gap of figure **(4.2.5.1.2)** lasted for more than a day (25th – 26th November 2006). Finally a third example is presented in figure **(4.2.5.1.3)**.

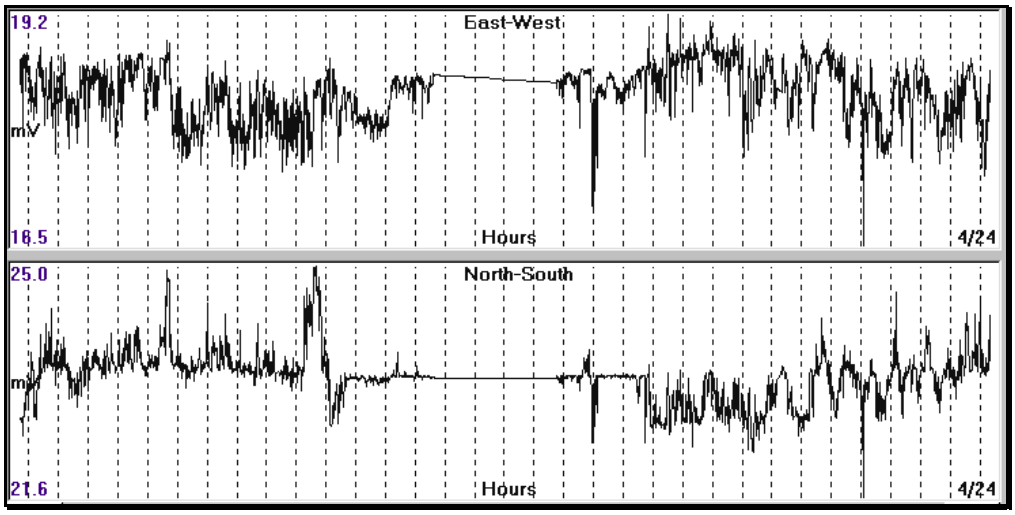

Fig. 4.2.5.1.3. "Missing data" and their linearly, interpolated values are presented, which were used to bridge the corresponding data gap. Date of gap recording, 16th January 2007, at Pyrgos **(PYR)** monitoring site.

The procedure, which is followed, in order to fill the data gap, does affect the "short wave length", electrical signals, recorded, with period of some hours the most. In practice, this data gap time period is replaced by a "noise free", new data set. However, it does not change the character of the entire data set, in the long wave length domain and therefore, does not affect the procedures which are applied for the epicentral area determination which deals, mainly, with much more longer periods.

Consequently, the error, which is introduced, on the data set by this type of “data preprocessing”, ranges from “negligible” to almost “zero”.

4.2.5.2. Noise rejection methodologies and filtering applied on data sets.

The time data series of electrical, potential which are registered and edited, so far, consist of any seismic, precursory, electrical signals, if these do exist, contaminated, by industrial or anthropogenic noise, any kind of superimposed, trends, on them and of any type of signals, induced, by the ionospheric activity. Therefore, it is very important to separate from each other, before any use of them is made for any earthquake prediction attempt.

The procedure which is used for this type of processing is called “filtering”. Filtering is distinguished, generally, to “low pass”, in which only low frequencies, below a certain value, pass through the used filter, “band pass”, in which a certain “frequency band” is allowed to pass through the filter and “high pass”, in which only high frequencies, above a certain value, are allowed to pass.

Filtering implementation is made through various methodologies such as:

4.2.5.2.1. Running a moving average (equally weighted or not).

This is the most basic scheme, which is used and corresponds to the implementation of a “low pass” filter. In the case of its application in a **differential operator mode** it corresponds to a “high pass” filter. A combined operation of “low-pass” and “high-pass” filters, sequentially, on the same data set, after appropriate selection of the filters characteristics, produces a band-pass output.

4.2.5.2.2. Polynomial fitting.

A different approach, for filtering implementation, is made through the use of polynomial, fitting to the data set. In this methodology, any data set of **N** equally, spaced data values can be transformed into an **N-1** order, polynomial function. The constant parameter of each polynomial term is evaluated, through a least square (LSQ) methodology, from the data values. If the **Z** transformation is taken into account, then, by omitting higher order terms of the calculated polynomial, the reconstructed data series corresponds to a new data set that contains only the lower terms of the frequency content of the original data. It is in practice a “low-pass” filtering operation.

4.2.5.2.3. Fast Fourier Transform (FFT).

The method, which is mostly used by the scientific community, for any data filtering, is the traditional **Fast Fourier Transform (FFT).** In a very short description of this methodology, the original data are, initially, converted into its frequency spectrum. A filter (of any kind), is used to retain the frequency band of interest, rejecting the entire, unwanted spectrum. Finally, from the retained frequency spectrum, the filtered data, in time domain, are reconstructed. A detailed analysis of the topic was presented by Bath (1974) and Kulhanek (1976).

In this case of data, which are recorded by the monitoring sites, in this earthquake prediction application, extensive use of the FFT methodology is made in order to separate the various oscillating components of the Earth’s electric field, which are triggered by the lithospheric, tidal oscillation. Below are some examples of the use of the FFT procedure on real data.

The first example **(fig. 4.2.5.2.3.1)** represents the application of a “low-pass” filter on the time data set of the Earth’s electric, EW component, registered, by **PYR** monitoring site.

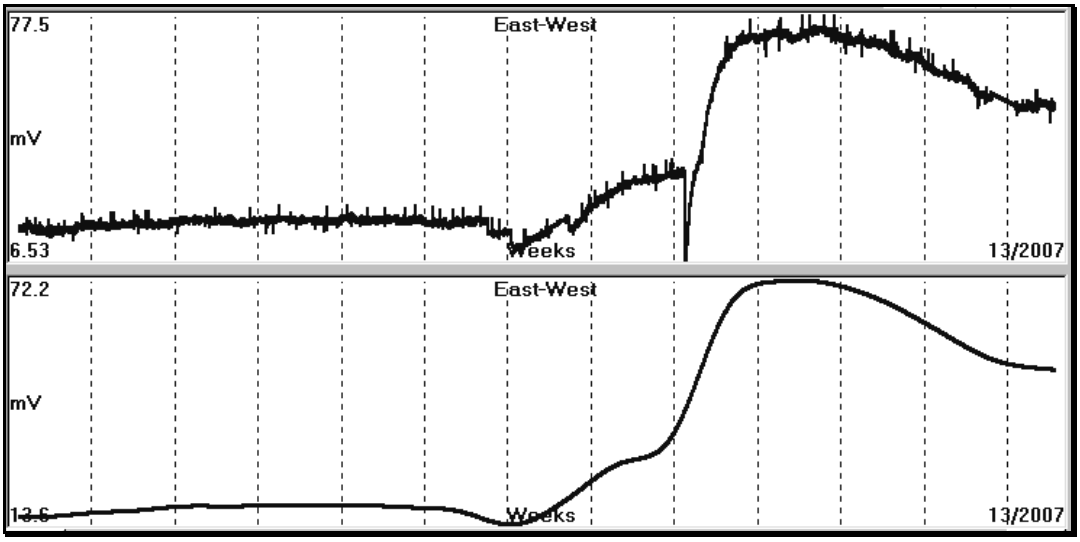

Fig. 4.2.5.2.3.1. "Low-pass" filtering of data, recorded by **PYR** monitoring site, for the period 1st January to 28th March, 2007 (**PYR** 070101 – 070328). Stop band of the filter = 10 days (bp=10days). The upper graph indicates the original data, while the lower graph indicates the "low-pass", filtered data.

Furthermore, the "low-pass" filtered data may be assumed as a long wavelength noise or trend. By subtracting this "noise" from the original data, the high frequency content of the registration, is enhanced. Moreover, by applying a "band-pass filter" on the original data, its oscillatory component can be derived. These operations are presented in the following figure **(4.2.5.2.3.2)**.

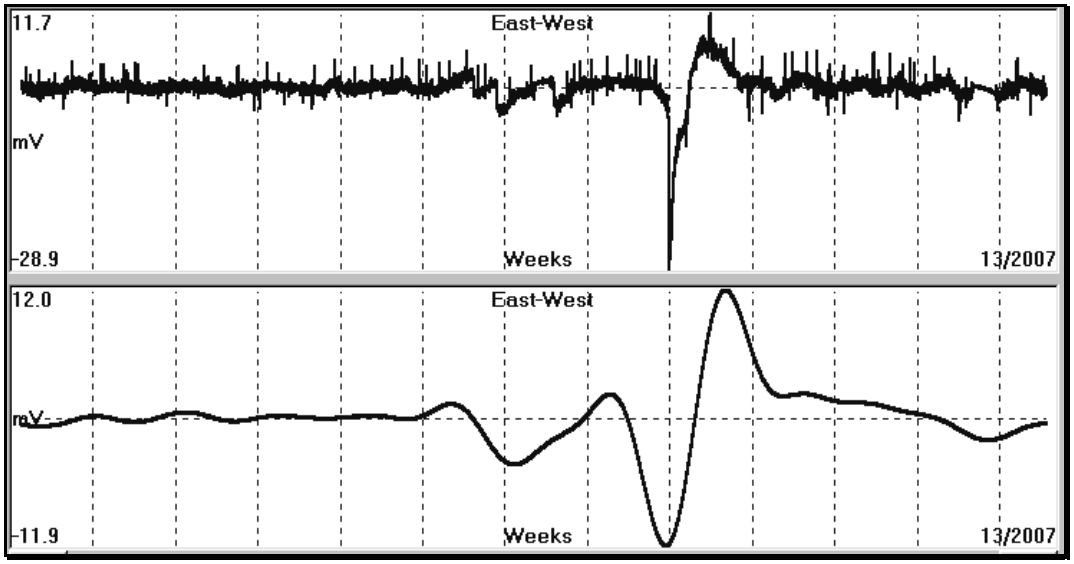

Fig. 4.2.5.2.3.2. The upper graph represents the "high-pass", filtered, original data, while the lower one shows the "band-pass" operation with a centered band (cpd = .1) at 10 days and bandwidth (bp=. 1) of 10 days, too. The recording period is 1st January to 28th March 2007 (**PYR**, 070101 – 070328).

The same methodology has been applied over a shorter time span of the original recording, but with a different bandwidth. In this case, the chosen parameters are: pass-band center = 1 day, with a bandwidth of half (0.5) of a day. The attempt is to identify, any one-day

period, oscillatory component of the Earth's electric field. This is illustrated in the following figure **(4.2.5.2.3.3)**.

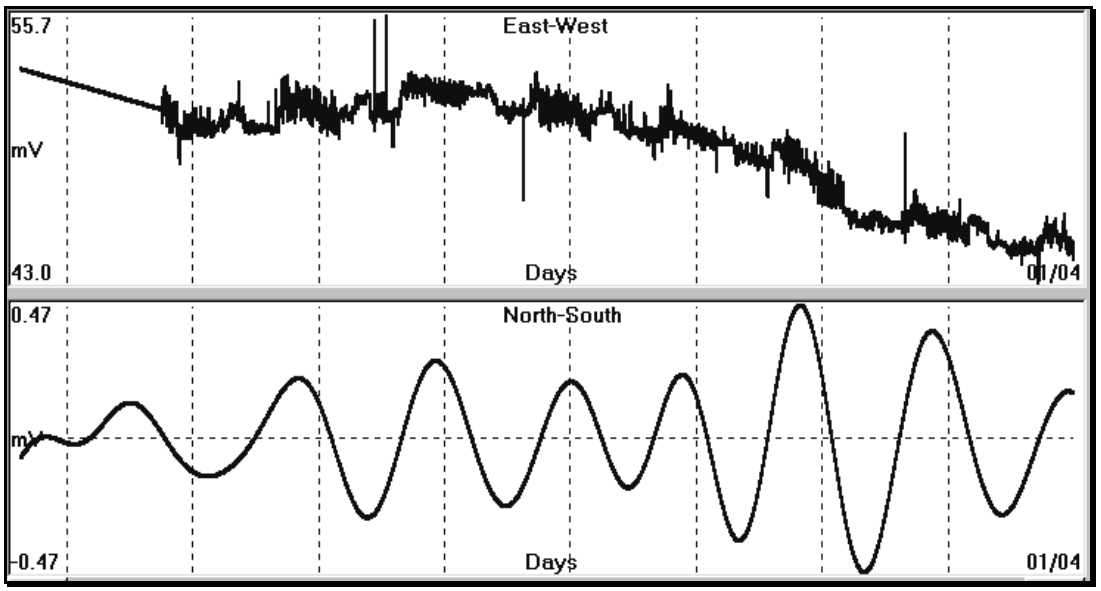

Fig. 4.2.5.2.3.3 The upper graph represents the original data, while the lower one the corresponding, oscillatory component of the Earth's electric field, identified, by the use of a "band-pass" filter, with a center frequency that corresponds to one day's period and a bandwidth of half (0.5) of a day (data recorded by **PYR** monitoring site, **PYR** 070325 – 070401).

The methodology was used for the "pre-whitening" of the original data, in a very similar way. This operation was performed after having chosen appropriate parameters for the filters, so that "white noise" will be eliminated from the original data. The center of the band-pass filter was chosen as 24 hours, while the band-pass of it, was set to 12 hours. This operation is demonstrated in the following figure **(4.2.5.2.3.4)**.

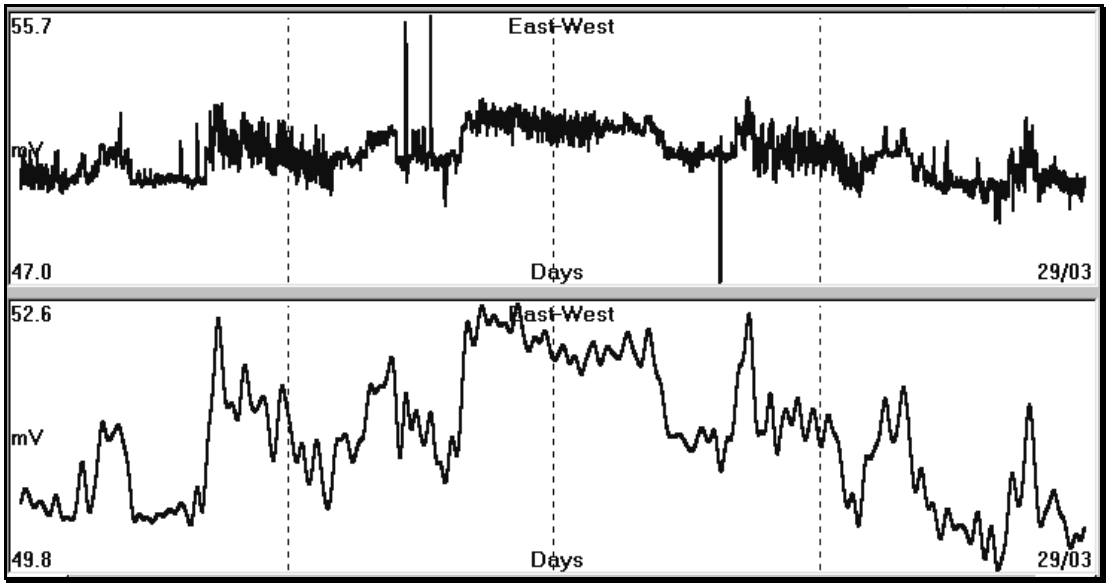

Fig. 4.2.5.2.3.4. "Pre-whitening" operation of the original data, recorded, for the period 26th March to 29th March, 2007 by **PYR** monitoring site (**PYR** 070326 – 070329). The center of "bad-pass" filter was set at 24 cycles per day; the bandwidth was set at 12cycles per day.

If the previous results are combined in a differential mode, then the “white-noise” frequency content of the original recording is obtained. This is demonstrated in the following figure **(4.2.5.2.3.5)**.

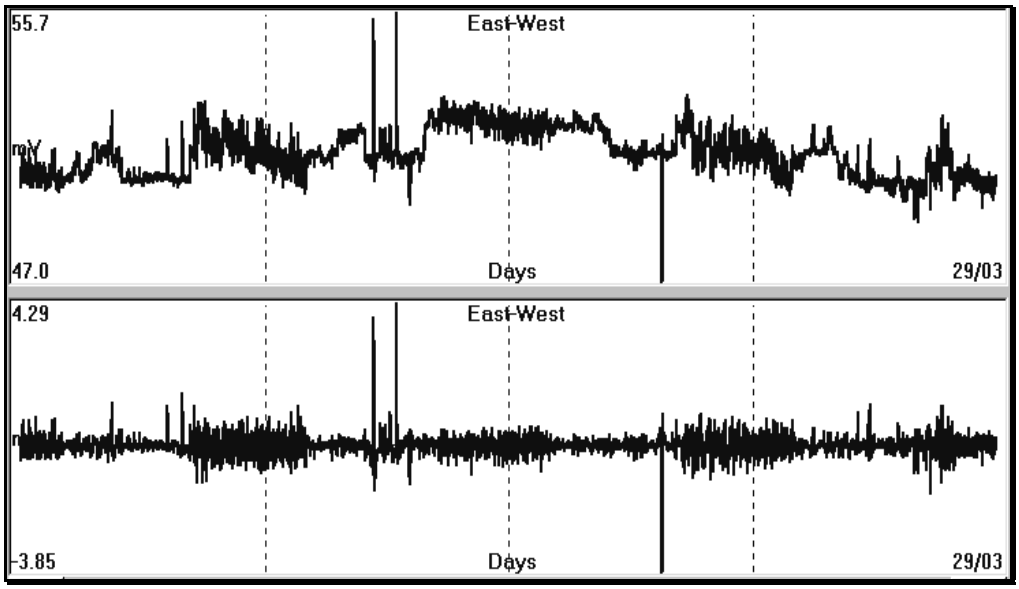

Fig. 4.2.5.2.3.5. The upper graph indicates the original data, while “white noise” content of the original recording is indicated in the lower graph (data recorded by **PYR** monitoring site, **PYR** 070326 – 070329). The center of band-pass filter was set at 24 cycles per day, the bandwidth was set at 12cycles per day.

The “pre-whitening” procedure was applied on a part of a recording which contains an SES signal. The **SES** signal, which was observed, on 4th March, 2007 on the recording of **HIO** monitoring site, is superimposed on an “anomalous” background noise. The “white noise” (and the **SES,** too) was eliminated, so that only the background noise is present. This is demonstrated in the following figure **(4.2.5.2.3.6)**.

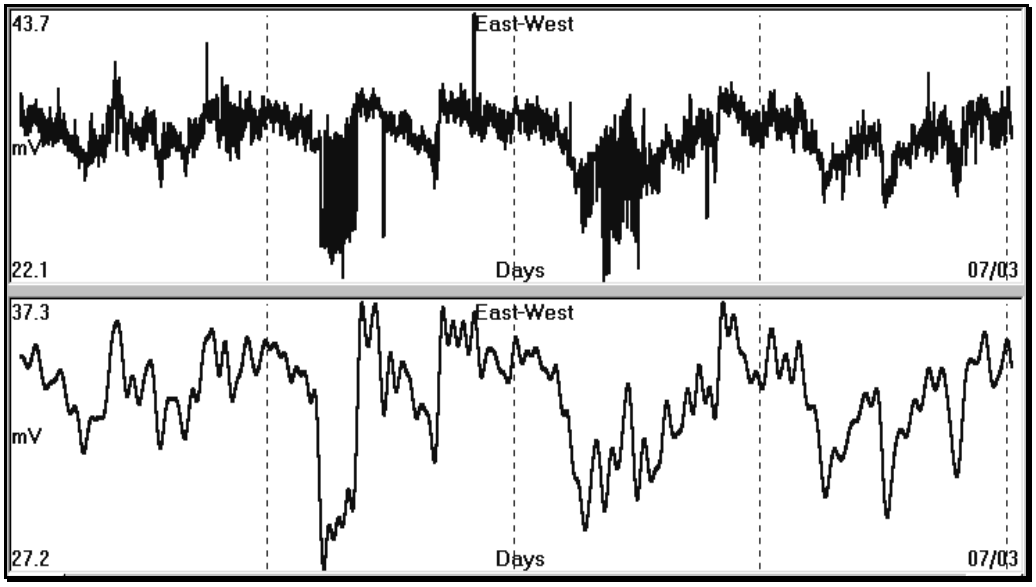

Fig. 4.2.5.2.3.6. The upper graph represents the original data with the **SES** present on 4th March, 2007, while the lower graph indicates existing noise (data recorded at monitoring site, **HIO** 070303 – 070306). The center of band-pass filter was set at 24 cycles per day; the bandwidth was set at 12cycles per day.

The latter is subtracted from the original data and the result indicates an **SES** signal, free from any "zero-level" irregularity. This is presented in the next figure **(4.2.5.2.3.7)**.

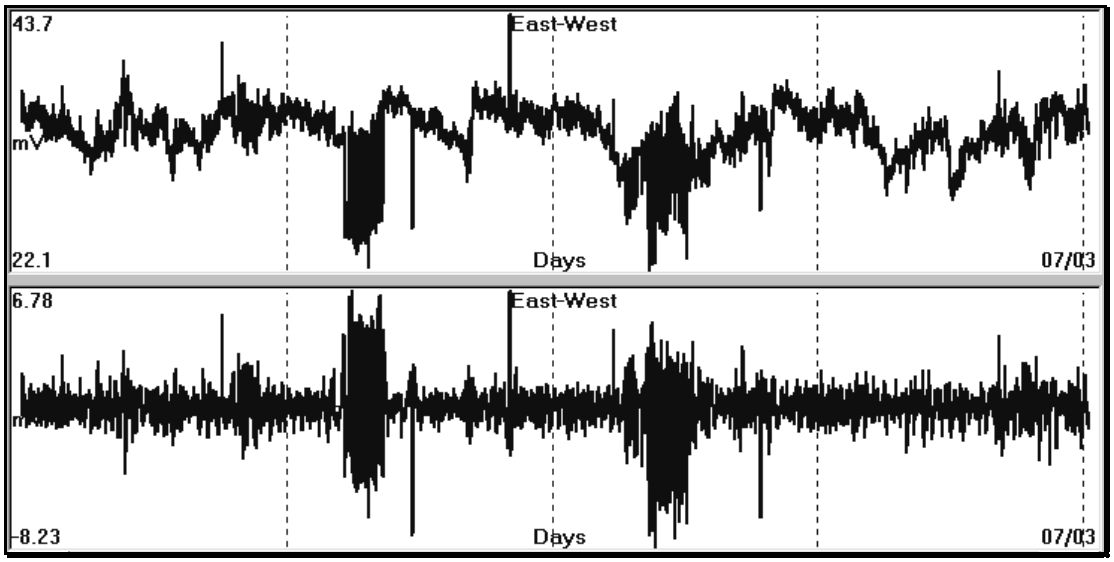

Fig. 4.2.5.2.3.7. The upper graph represents the original data, while the lower graph indicates the result of the filtering operation (data recorded by **HIO** monitoring site, (**HIO** 070303 – 070306). The center of band-pass filter was set at 24 cycles per day and the bandwidth was set at 12cycles per day.

A slightly different approach was followed by Varotsos and Lazaridou (1991), aiming to isolate **SES** signals from a noisy recording. The recordings of two different, in length, "in line" dipoles, were used in a differential mode. The, resulted, data were drastically "cleaned" from the anthropogenic noise, which was present, in the recording area.

In any case, the tools and the methodologies for any type of data filtering do exist. What must be pointed out is the following: **differential methods act as high-pass filters and therefore, long wavelength components of the processed, electrical signals data, are highly attenuated.** This corresponds to large loss of information useful for the determination of the epicentral area, as it will be shown later on. The opposite is achieved by integration, which performs as a "low-pass" filter (Thanassoulas, 1991). In this case, **SES** electrical signals, considered, as high frequency components of the registered, electrical field, are totally rejected (considered as noise) from the processed recordings.

4.2.5.2.4. Magnetotelluric impedance tensor.

The methodologies which have already been presented are based on the processing of the data itself, with an appropriate filter, after having defined what "noise" is and what is "**signal**". In this case, there is not any discrimination made, as far as it concerns the origin or the cause of the induced noise. In the specific case, of the noise, induced, through the ionospheric activity, an entirely different methodology was developed: that is the "**Magnetotelluric Impedance Tensor**".

Generally, ionosphere induces currents in the ground. These currents generate potential fields which can be analyzed into orthogonal components $\mathbf{E_{EW}}$ for the **E-W** and $\mathbf{E_{NS}}$ for the **N-S** direction. These, ionospherically induced, potentials can be calculated through the use of the **(T)** transfer function, which relates the magnetic fluctuations of the Earth's magneric field (**Hx, y, z,** components), with the induced on the ground potentials $\mathbf{E_{EW}}$ and $\mathbf{E_{NS}}$ and the resistivity and tectonic structure of the Earth at the place of the site of investigation. Chouliaras (1988), presented the details of the methodology and its application on recordings, referred, to **VAN**

monitoring sites. The procedure, which is followed, is a simple subtraction of the induced "noisy", electrical, ionospheric, theoretical components from the actual recordings which are obtained at the same monitoring site. The resulting output of this procedure is considered, as free, from any ionospheric signal contamination.

The problem of noise contamination of any type of data is generally presented in the following figure **(4.2.5.2.8)**. The registered data are presented in terms of their frequency spectrum to facilitate the analysis that follows. It is assumed that the signal of interest is present in terms of frequency content in the "**band of interest**", while a wide spectrum of noise spans allover the recording spectrum. The frequency band which represents the signal of interest is shown in figure **(4.2.5.2.8)** with right, inclined, dashed lines, while the noise spectrum is shown with left, inclined, solid lines.

The problem, which is posed, is as follows: how is it possible to extract the signal of interest from the contaminated, noisy data. The methodologies available, to date are: low-pass filtering, high-pass filtering or their combination in terms of band-pass filtering. The philosophy behind these operations is the same, no matter which methodology is used. A suitable, band-pass filter will be used for the particular case in figure **(4.2.5.2.8)**.

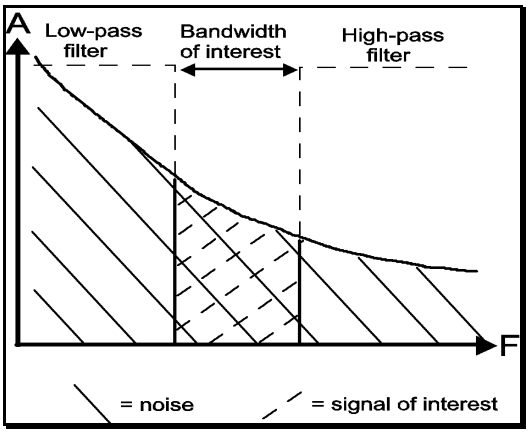

Fig. 4.2.5.2.8. Schematic presentation of the frequency spectrum of a time series data recording, which has been contaminated by a wide spectrum type of noise.

What is clear, from figure **(4.2.5.2.8),** is that the application of a band-pass filter upon the data will extract the data of interest, but at the same time it will retain the content of noise, which coincides with the band of interest. Therefore, the output of any band-pass filter, even of a theoretical one, will retain a certain degree of noise. If the signal to noise ration (SNR) of the original recording is large enough, then there might present no problem at all. In case when SNR is very small, then the problem becomes serious. The signal of interest is completely masked by the noise and the entire recording becomes, probably, useless.

This problem is usually faced in the recordings of the Earth's electric potential, when preseismic, electrical signals are to be detected. An example of such a recording is presented in the following figure **(4.2.5.2.9)**.

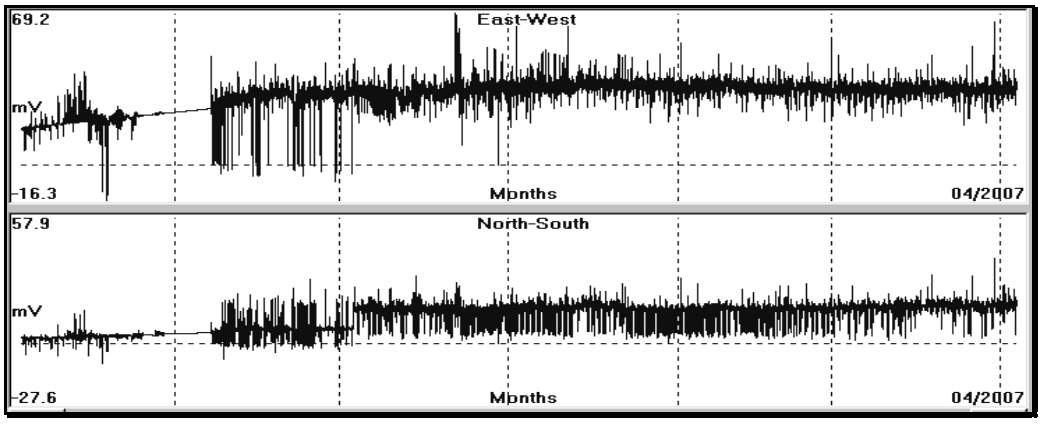

Fig. 4.2.5.2.9. Presentation of the EW, NS components of the Earth's electric potential registered, by **HIO** monitoring site, during the period 4th October, 2006 to 3rd April, 2007 (**HIO** 061004 – 070403).

A close inspection of the recording indicates that the Earth potential data have been contaminated by noise, which consists mainly of rectangular pulses of very short duration. The application of any of the previously, referred, filters, probably may eliminate the electrical pulses, but at the same time they will affect the data of interest, too. The target of a successful, filtering operation is to eliminate the noise, without affecting the signal of interest, at all. It is evident that a completely different approach must be invented and used, as well. A first reaction of the reader could be such as: it is impossible!! Well, is it?

4.2.5.2.5. Noise injection methodology for time series data filtering.

This methodology, in its principle, although it may seem bizarre, is borrowed by the medical science. Let us assume that a patient is ill, because of an infection by a virus. The pathologist, after having studied the symptoms of the illness, advises the patient to take antibiotics. The level of antibiosis is controlled by the course of the illness. If the patient does not get better, then the level of antibiosis increases, until he becomes totally healthy. The kind of antibiosis depends on the type of virus.

This common, medical procedure will be translated now into the filtering methodology to be applied on a time series data set. The data set corresponds to the patient. The noise contamination corresponds to the illness and the noise type corresponds to the virus. The scientist (physicist, seismologist, geophysicist e.g.) corresponds to the pathologist. What is still missing is the type of antibiosis to be used and its level that will make the data "healthy" again.

The noise, which is observed in figure **(4.2.5.2.9),** consists of electrical spikes of small duration. Their origin is not important at the present time, but their presence affects badly any preseismic, electrical signal which could be present in this recording. These electrical spikes are considered as **"Dirac delta functions"**, which are rectangular pulses, of an infinitesimal width, and unit area beneath each pulse (Kulhanek, 1976). Each spike can be represented by an infinite number of sinusoidal components of unit amplitude, in phase, at the time of spike occurrence. The latter is illustrated in the following figure **(4.2.5.2.10)**.

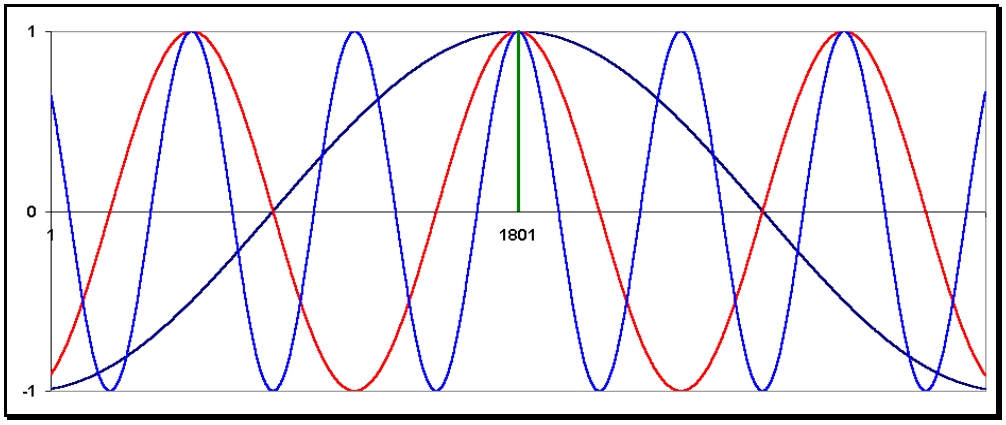

Fig. 4.2.5.2.10. The "**Dirac delta function**" at time t = 1801 minutes and its first three most significant components.

It is evident, that the frequency components of any electrical spike content in the data set, which fall into the bandwidth of interest, will not be affected at all by the use of any type of filter, which could be used. These spike's frequency components, which are present in the bandwidth of interest, still distort the original signal of interest.

Since the traditional, filtering techniques fail to solve the problem, the medical treatment analogy will be followed (!). What is needed, immediately, is an antibiotic. This is the same, exact "**Dirac delta function**", with opposite sign, which corresponds to a specific, electrical spike. If a data spike of opposite sign and of the same amplitude is injected in the data series at the same time of the spike occurrence, then the entire frequency noise spectrum, caused by, the spike itself only, will

be eliminated. Consequently, only the signals of interest will remain in the band of interest. What is still open in questioning is the amplitude of the injected spike. Since, there is no clue about the noisy spike original amplitude, a range of different amplitudes is used and the resulted, “filtered” data form a family of possible, “noise free” registrations.

The entire procedure is demonstrated through the use of a synthetic example. A sine wave was generated, with amplitude of 2 units peak to peak (p-p), which is presented in the following figure **(4.2.5.2.11)**.

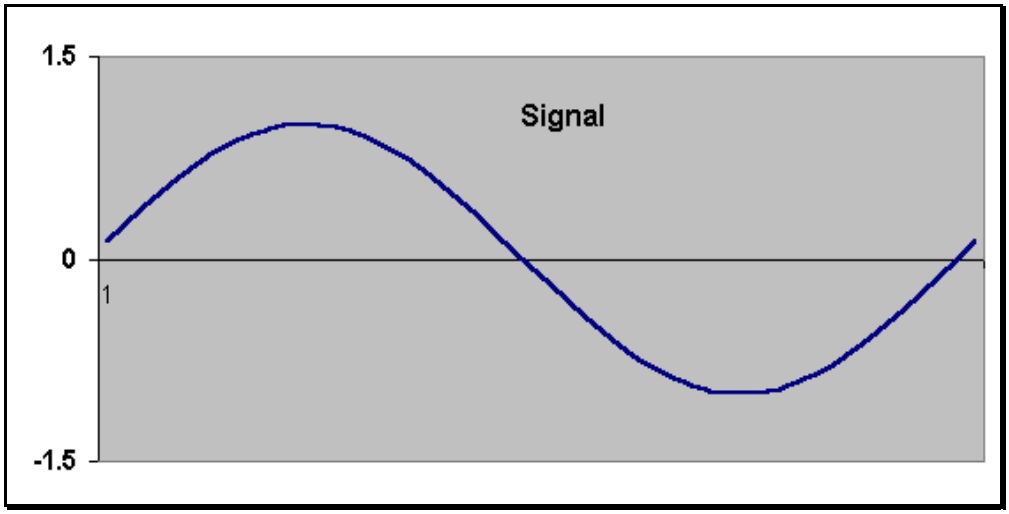

Fig. 4.2.5.2.11. Schematic presentation of a synthetic sinusoidal signal, with amplitude of 2 units p-p.

The sinusoidal signal of figure **(4.2.5.2.11)** will be “contaminated” by a noise of about 38 units p-p. The noise amplitude was generated by a random number generator for the same time span, as for the sinusoidal wave. The form of the calculated noise is shown in the next figure **(4.2.5.2.12)**.

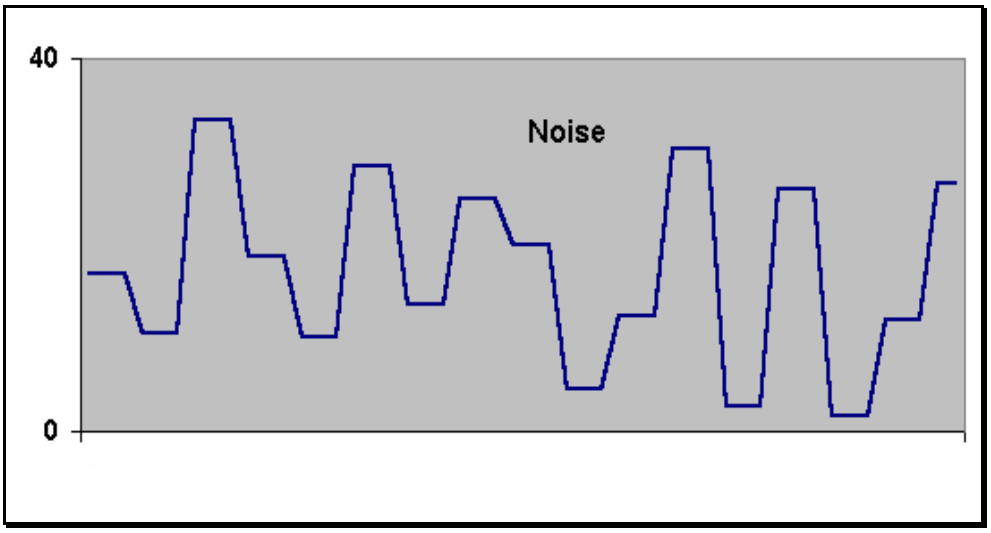

Fig. 4.2.5.2.12. Presentation of noise, generated for the same time span, as in figure **(4.2.5.2.11),** by a random procedure.

The **SNR (p-p)** of the sine wave amplitude to the noise amplitude is: **SNR = -26 db.** The sine wave and the noise are combined in one data series, which is presented in the following figure **(4.2.5.2.13).**

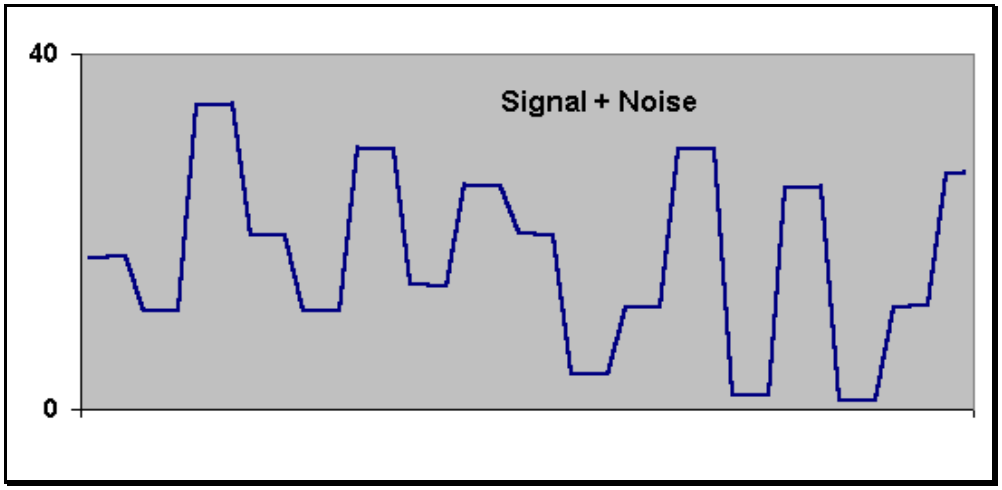

Fig. 4.2.5.2.13. Synthetic signal generated by a sine wave **(fig. 4.2.5.2.11)** and random noise **(fig. 4.2.5.2.12).**

A comparison between the random noise, illustrated in figure **(4.2.5.2.12)** and the synthetic, noisy data, presented in fig. **(4.2.5.2.13)** shows, practically, no difference at all. This is caused by the fact that the SNR is very small thus, the noise, practically, masks completely any visible sine wave.

Next step towards the recovering of the signal of interest (sine wave) is to apply the methodology, which has already been presented. From the various "Dirac delta functions" amplitudes, used, the one with amplitude parameter **(p):**

p = 1

generated the best results, shown in the following figure **(4.2.5.2.14)**.

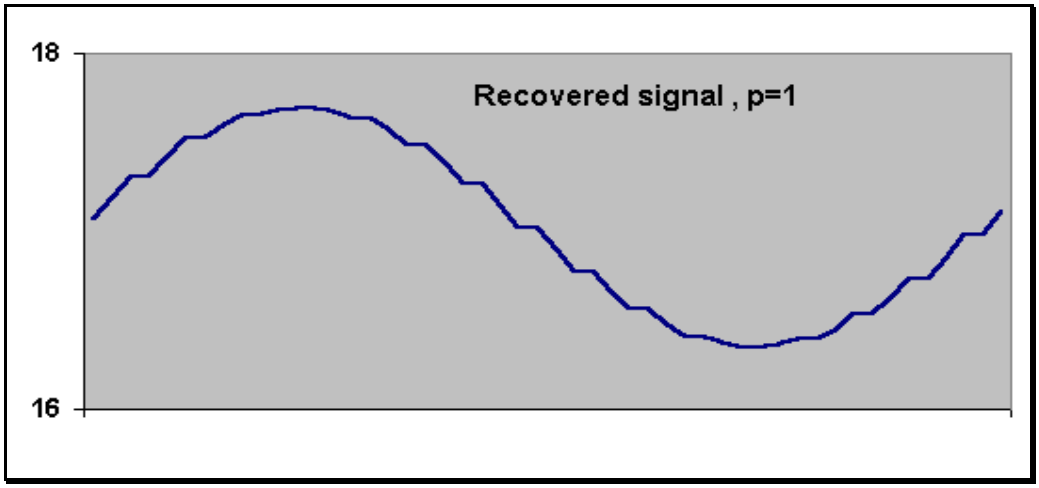

Fig. 4.2.5.2.14. The recovered signal, from noisy data of figure **(4.2.5.2.13)** is presented, after the application of the "noise injection methodology".

It is evident that, the recovered signal resembles, pretty well, the original signal, which is used for the purpose of demonstration and refers to the "noise injection methodology". The already presented noise filtering methodology was applied on real data registered in **HIO** monitoring site, for a period of six (6) months (4th October, 2006 to 3rd April, 2007). The **(p)** parameter, used, ranges in the span **p = .625 to 40**. The examples, presented, refer to both **EW** and **NS** components of the Earth's electric potential. The different **(p)** values, which are used, are also presented in ascending order.

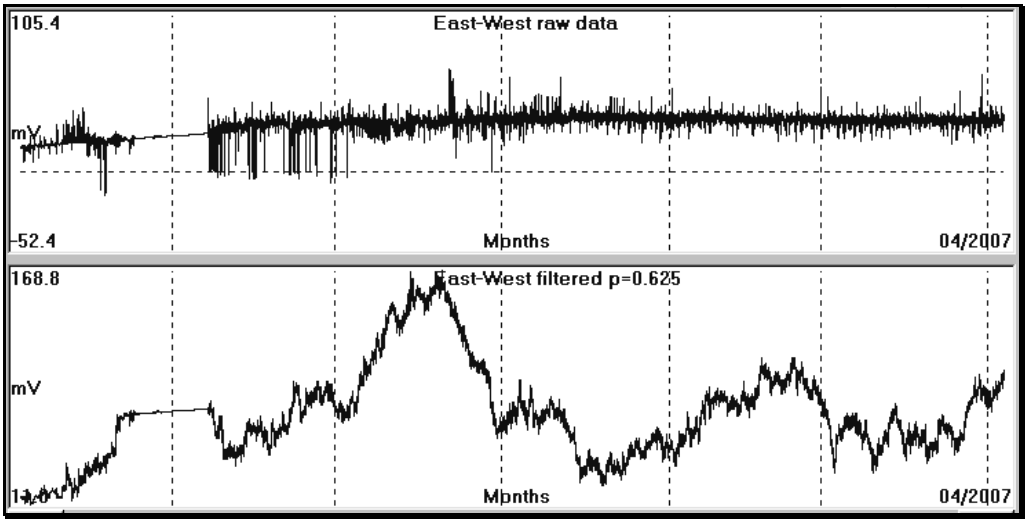

Fig. 4.2.5.2.15. **HIO, EW** data, processed, by the noise injection methodology, using **p = 0.625**

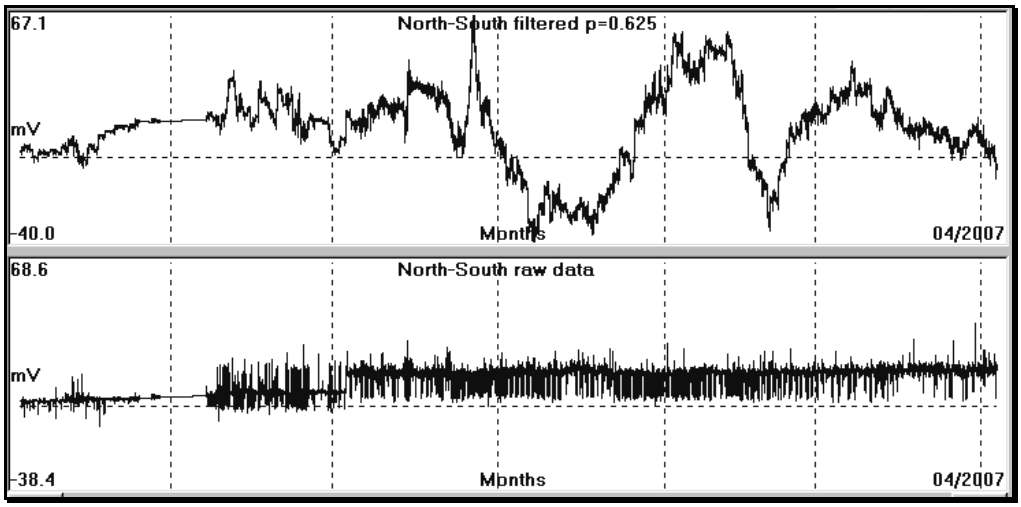

Fig. 4.2.5.2.16. **HIO, NS** data, processed, by the noise injection methodology, using **p = 0.625**

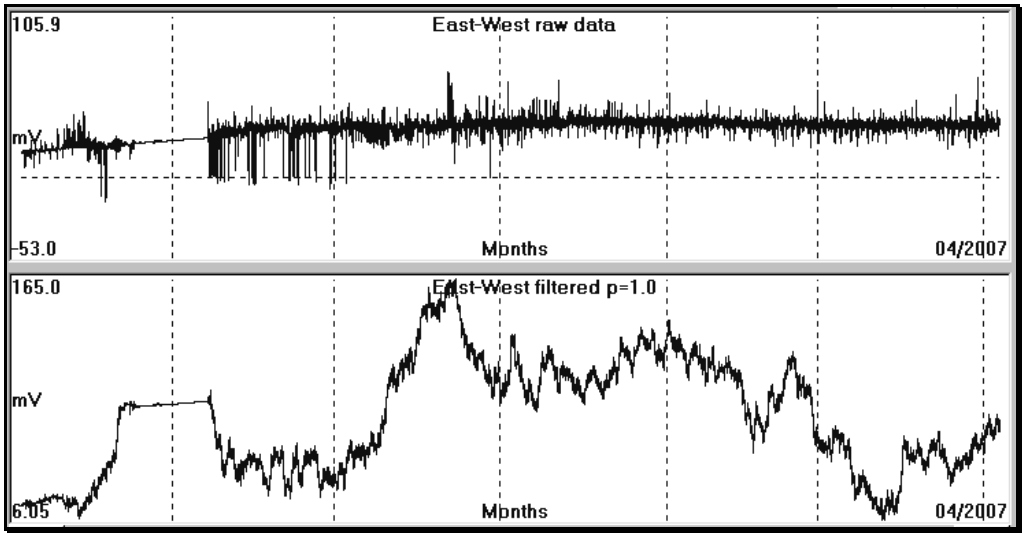

Fig. 4.2.5.2.17. **HIO, EW** data, processed, by the noise injection methodology, using **p = 1.0**

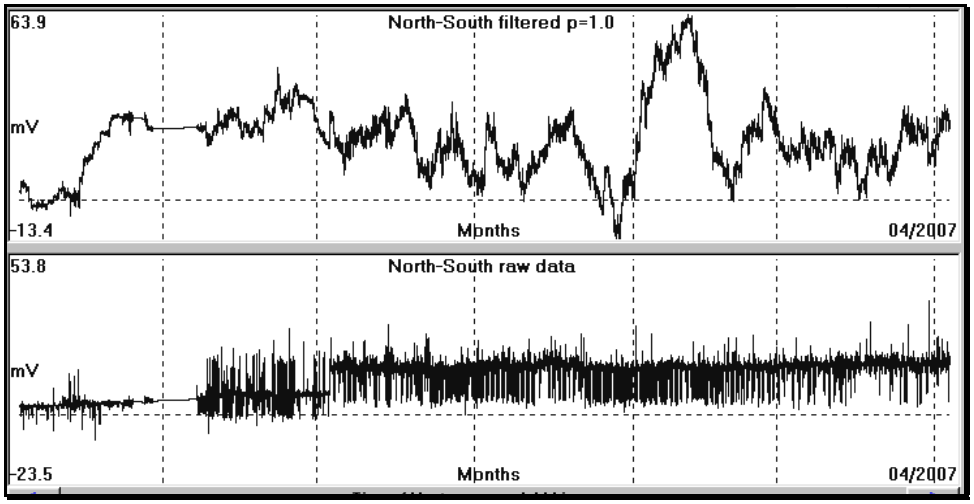

Fig. 4.2.5.2.18. **HIO, NS** data, processed, by the noise injection methodology, using **p = 1.0**

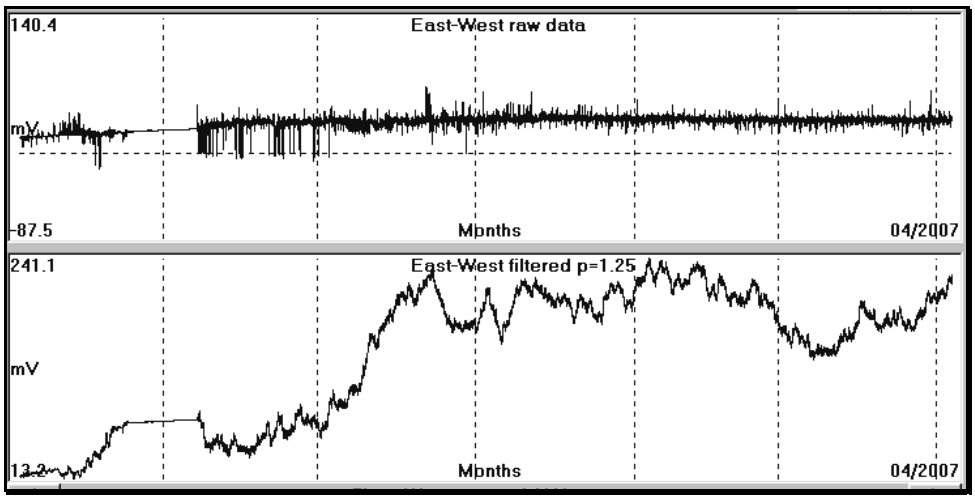

Fig. 4.2.5.2.19. **HIO, EW** data, processed, by the noise injection methodology, using **p = 1.25**

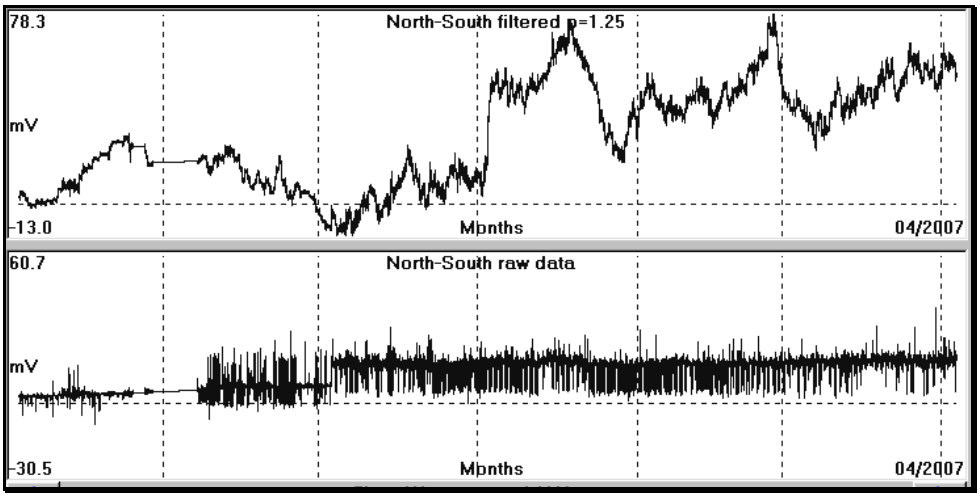

Fig. 4.2.5.2.20. **HIO, NS** data, processed, by the noise injection methodology, using **p = 1.25**

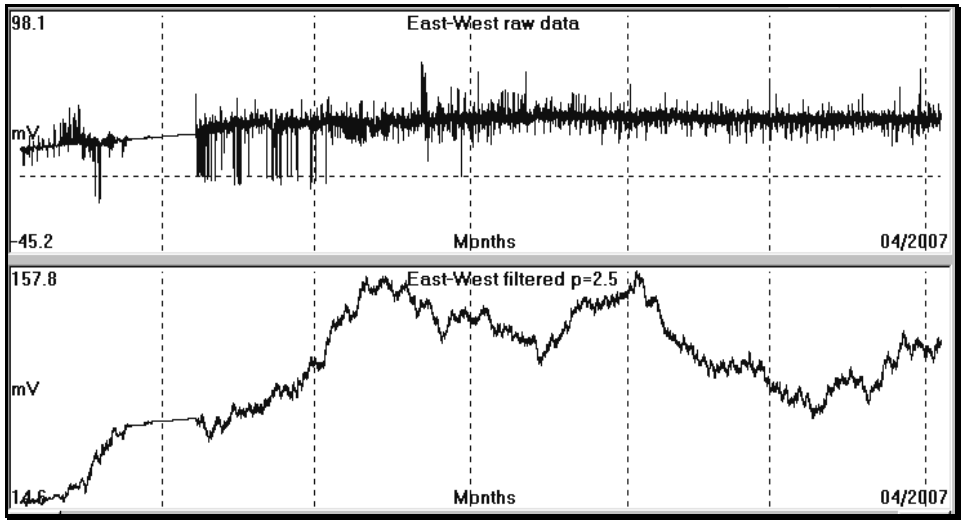

Fig. 4.2.5.2.21. **HIO, EW** data, processed, by the noise injection methodology, using **p = 2.5**

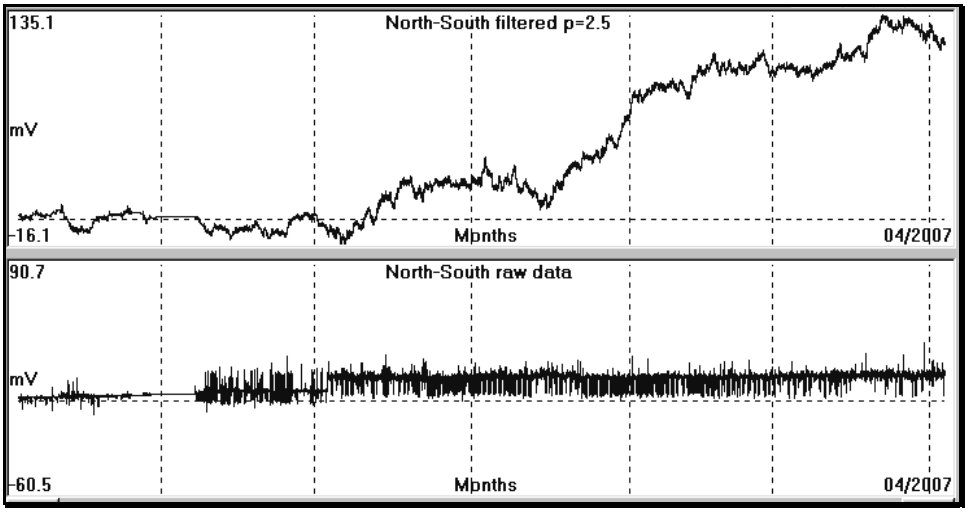

Fig. 4.2.5.2.22. **HIO, NS** data, processed, by the noise injection methodology, using **p = 2.5**

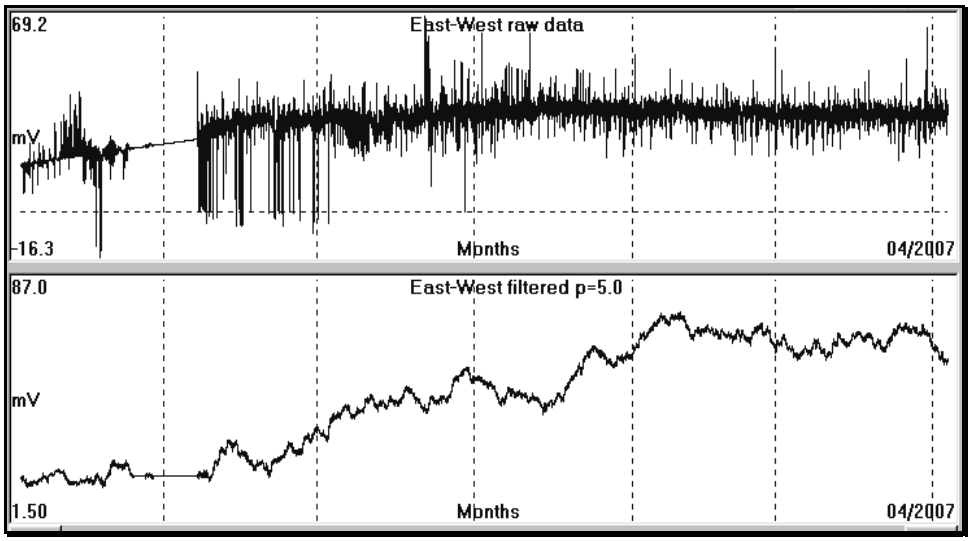

Fig. 4.2.5.2.23. **HIO, EW** data, processed, by the noise injection methodology, using **p = 5.0**

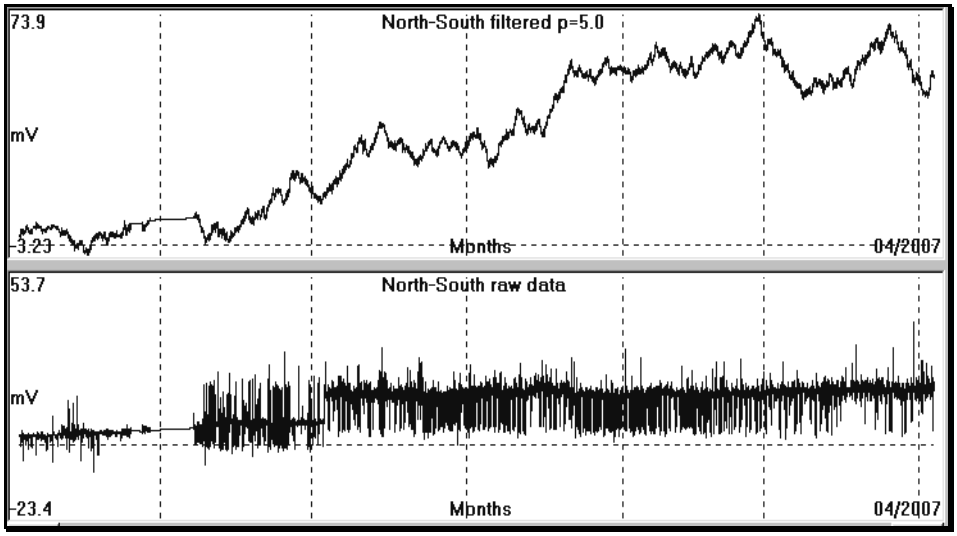

Fig. 4.2.5.2.24. **HIO, NS** data, processed, by the noise injection methodology, using **p = 5.0**

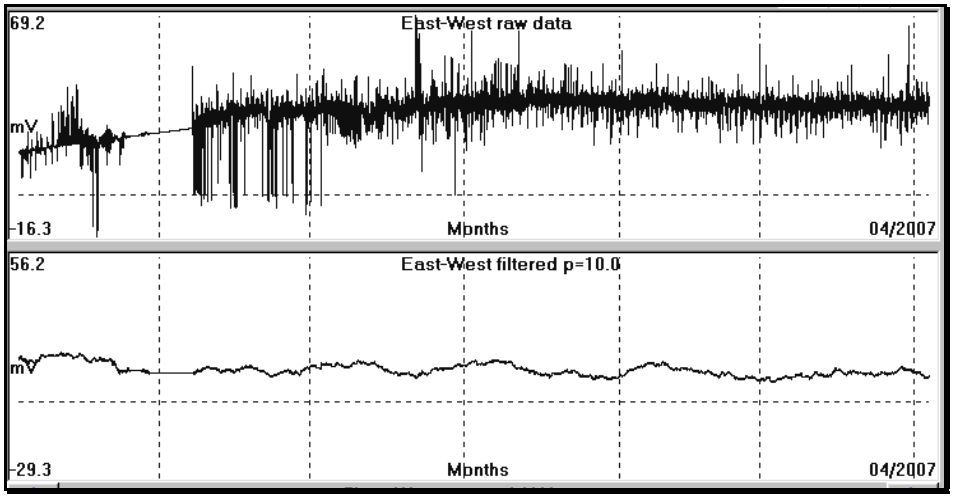

Fig. 4.2.5.2.25. **HIO, EW** data, processed, by the noise injection methodology, using **p = 10.0**

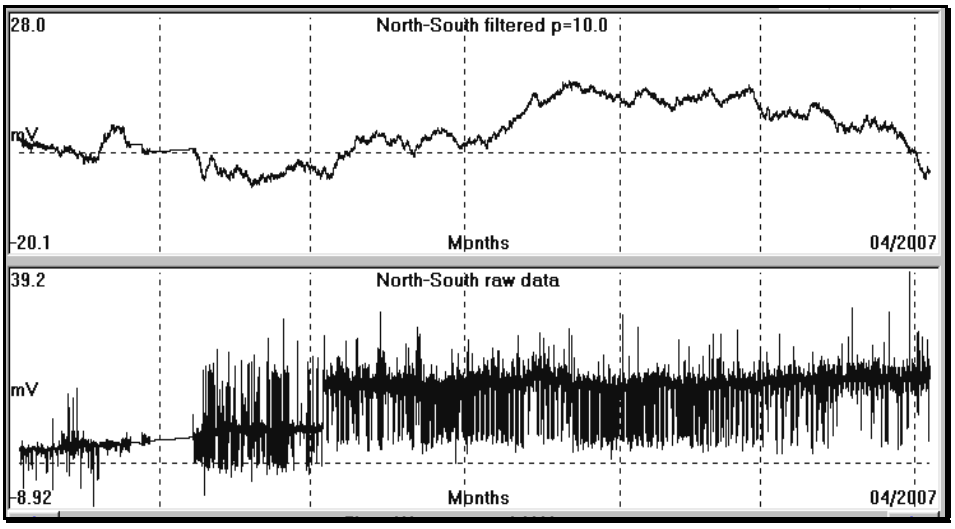

Fig. 4.2.5.2.26. **HIO, NS** data, processed, by the noise injection methodology, using **p = 10.0**

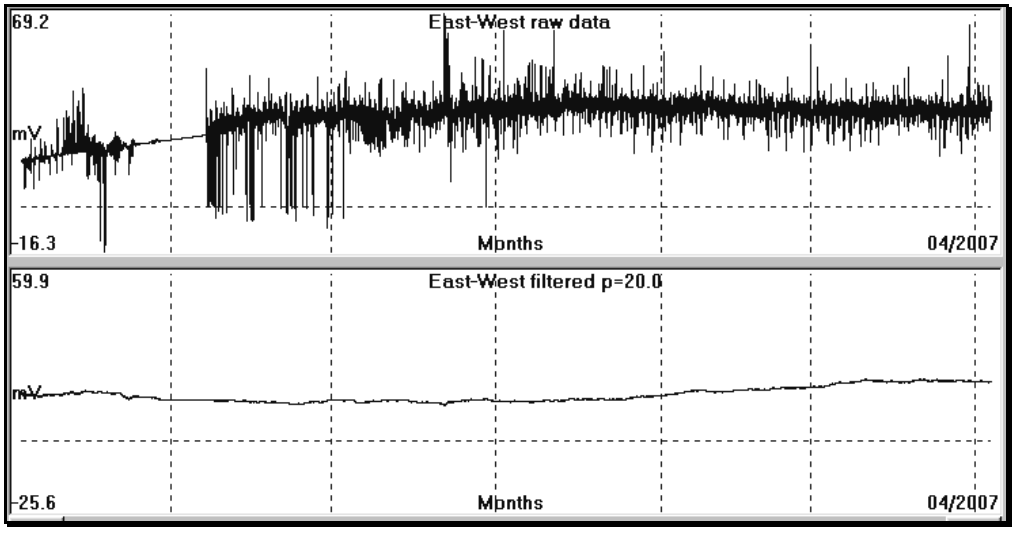

Fig. 4.2.5.2.27. **HIO, EW** data, processed, by the noise injection methodology, using **p = 20.0**

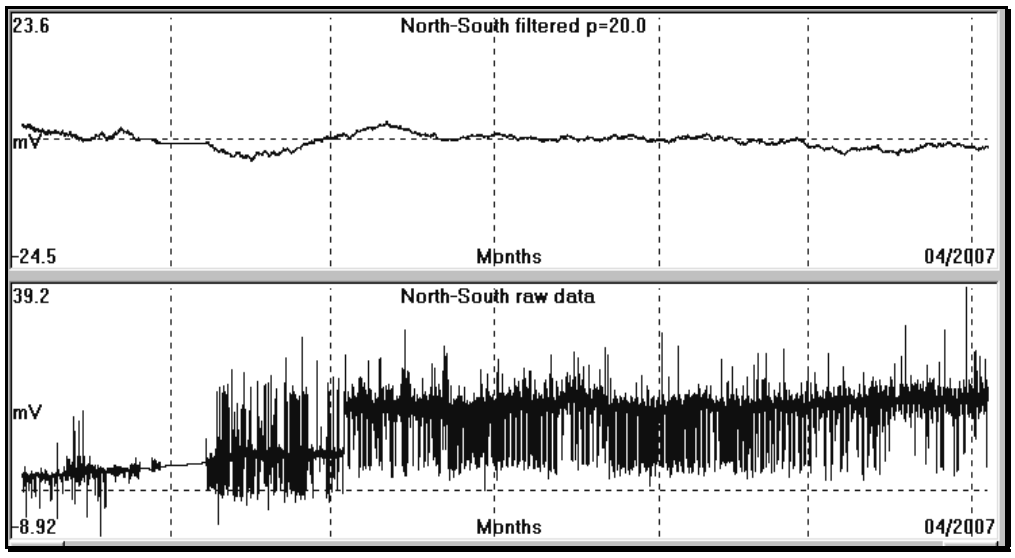

Fig. 4.2.5.2.28. **HIO, NS** data, processed, by the noise injection methodology, using **p = 20.0**

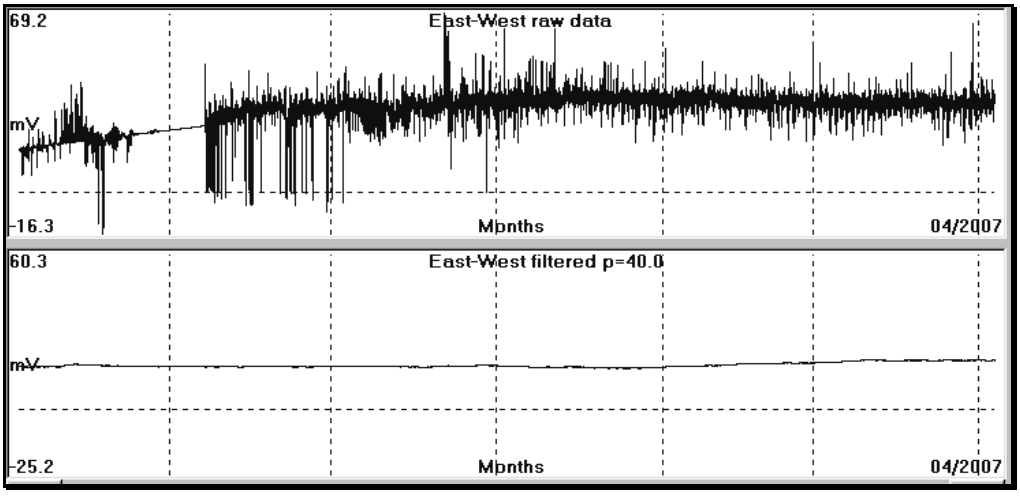

Fig. 4.2.5.2.29. **HIO, EW** data, processed, by the noise injection methodology, using **p = 40.0**

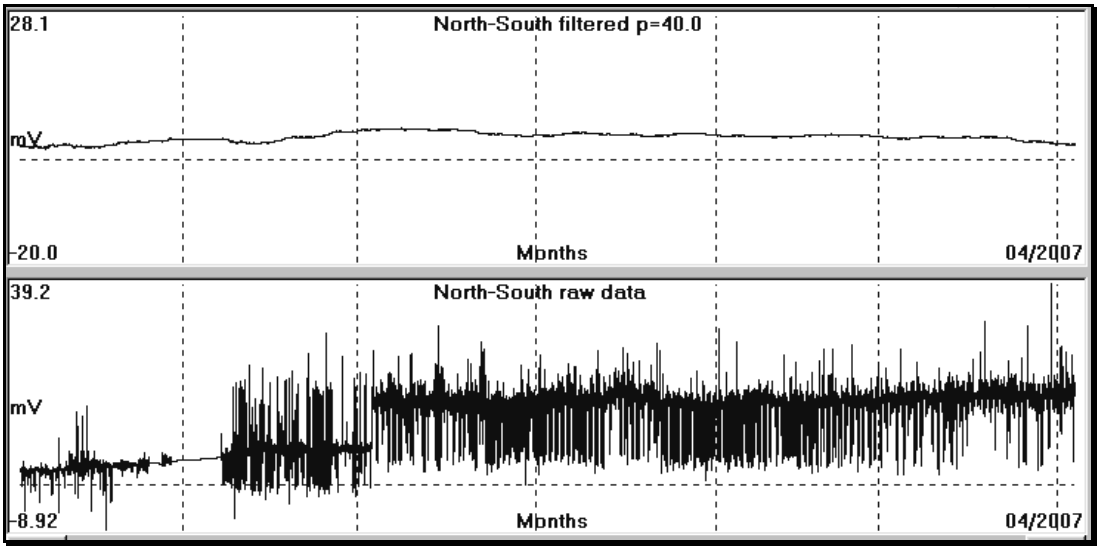

Fig. 4.2.5.2.30. **HIO, NS** data, processed, by the noise injection methodology, using **p = 40**

A comparison of the previous examples, in relation to the gradual increase of **(p)** parameter value, indicates that for very large **(p)** the noisy data set actually collapses to almost a straight line, in case of absence of any significant, anomalous, electrical signal.

Finally, the methodology of noise injection was applied on data, registered, long before two strong earthquakes. The first one is the one in IZMIT, Turkey (M = 7.5 R, 17th August 1999) and the second one is in MILOS, Greece (M = 5.6 R, 21st May 2002).

The electric potential, generated by IZMIT EQ focal area, was recorded by a single dipole in Volos, Greece, at a distance of 650km from the epicentral area. The raw data and the filtered ones are presented in the following figure **(4.2.5.2.31)**.

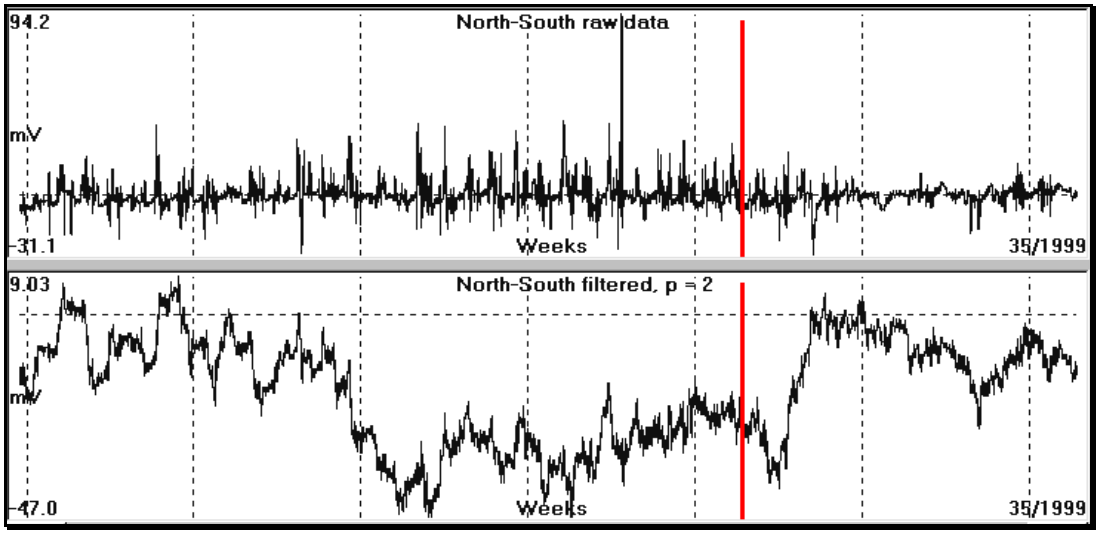

Fig. 4.2.5.2.31. Raw data (upper graph) and filtered by the noise injection methodology (lower graph, p=2), which correspond to **IZMIT** earthquake, are, presented. The red bar indicates the time of occurrence of **IZMIT** EQ.

The plateau-type signal (first derivative of the total potential generated) was recovered pretty well.

The second example, of MILOS EQ, is presented in the following figure **(4.2.5.2.32)**. A straight line fits, very well, with the raw data, presented, in the upper graph, while the filtered data (lower graph), is quite a different case.

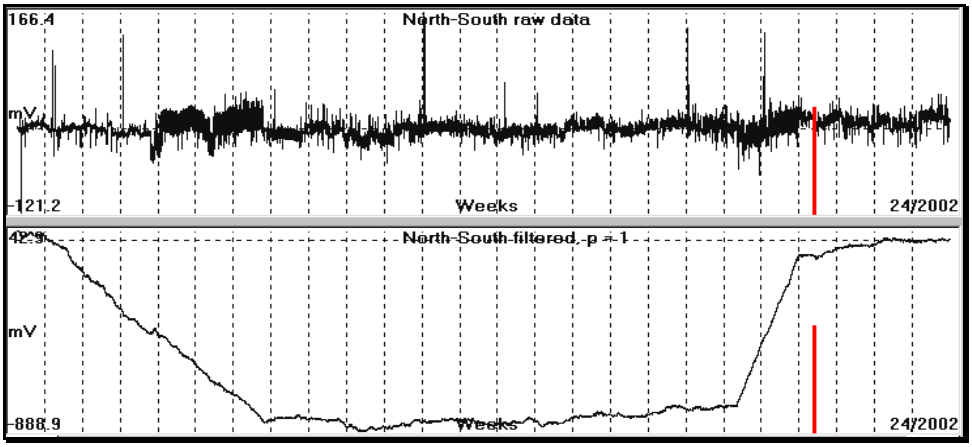

Fig. 4.2.5.2.32. Raw data (upper graph) and filtered by the noise injection methodology (p = 1, lower graph), which correspond to MILOS earthquake, are presented. The red bar indicates the time of occurrence of MILOS EQ.

In the case of MILOS EQ the preseismic electric signal lasted for more than twenty (20) weeks. In this case, too, the preseismic signal has the typical form of the first derivative of the total Earth potential, generated, by the physical mechanism at the focal region.

Both, already presented examples, suggest the activation in the focal area of a large-scale piezoelectric mechanism.

In conclusion, methodologies, for the effective filtering out of any noise which has contaminated any earthquake precursory, electrical signals, recorded on the ground and at any distance from the epicentral area, exist. The signal to noise ratio **(SNR),** which is present in these recordings, dictates the most appropriate methodology to be used.

4.2.6. Preseismic electrical signal identification.

The way of obtaining a continuous time data set from the registration of the Earth's electric field, which is observed on ground surface, has been demonstrated at the present time. More over this data set can be subjected to "pre-whitening operations" or any other type of filtering, so that it results in to a "clean" recording. So far, no assumption was made for the type of anomalous signals content of any data set. Therefore, any kind of signals, such as of anthropogenic origin, ionospheric origin and of seismogenic – tectonic origin, could be incorporated in any "cleaned" data set.

Consequently, the question, which arises, is: does a particular data set contain any precursory, electrical signals and if so, how is it possible to identify them?

It is not an easy task to answer this question. Actually, it takes knowledge of the insight of the physical mechanisms, which are activated each time during the preparation stage of an earthquake, which unfortunately, is not clear to the researchers, yet. Even if these physical mechanisms were known, still the problem exists of the variability of the mechanisms, triggered each time, in the same seismogenic area, and at different time periods. Consequently, the signature of the preseismic, electrical signal to be generated is still unknown.

Many researchers studied this specific problem, of the identification of the preseismic, electrical signals. Varotsos and Lazaridou (1991) used the **dV/dl = constant** criterion to compare potential values, registered, with short dipoles of different length at the same monitoring site; the preseismic, electric signal must appear simultaneously on the short and long dipoles of the stations, concerned; the **MT** noise can be distinguished in the recordings, since it is recorded simultaneously in all dipoles, in all monitoring sites; while, "the polarity and amplitude of the preseismic signal on the short and long dipoles must be compatible with a distant source assumption". More over, guidelines and examples were presented for the discrimination of preseismic, electrical signals from artificial noise and from magnetotelluric changes (Varotsos, 2005).

However, the latter criteria were strongly objected by Tzanis and Gruszow (1998).

The same problem was treated, in a differently approach, by Ozima et al. (1989). The Bayesian approach (Ishiguro 1981; Ishiguro et al. 1984) of the analysis of the data, related to crustal movements, was adopted and the observed Earth potential data were separated into four components: tidal, electromagnetically induced, trend and irregular component.

Thanassoulas (1991) used traditional Fast Fourier Transform (FFT) in order to identify very long period **(VLP)** signals, incorporated, in the recordings of the Earth's electric field, signals which were registered by the **VAN** group prior to Kalamata (15^{th} September 1986, Ms = 6.2R). In this work, anomalous signals of period less than a day were considered as "noise" of any kind and therefore, were completely rejected by the use of a low pass filter. The output of this filter was used, successfully, to determine the azimuthal direction of Kalamata EQ, in relation to the location of the recording station.

Cuomo et al. (1996) proposed a statistical method, to evaluate extreme events in earthquake precursory signals of electric nature. The occurrence probability of seismo-electrical anomalies is computed by means of a parametric time series approach. In a second step an autoregressive model, to describe the residual time series, is suitably identified and fitted to the data. Finally, parametric inference of extreme events is carried out on the basis of the selected model.

Enomoto et al. (1997) used a different approach for the characterization of pulse-like, geoelectric signals as being related to seismic activity. In this methodology the anomalous electrical signals are compared in turn with: a certain threshold level, simultaneous recording by more than one stations, presence of lightning, association of thunder clouds or radar echo, simultaneous presence of the signal in the VLF band. In a positive result, the signal is considered as a possible seismic precursor and is compared to any seismic activity at a threshold level of 5.5R.

Cuomo et al. (1998) investigated the time dynamics of geoelectric, precursory time series, using autoregressive models. The approach he uses allows information, to be obtained, on the geophysical system, which produces the electrical phenomena in seismic, active areas, when the only information about the time series comes from the time series themselves. It is based on two forecasting approaches: the global, autoregressive approximation and the local, autoregressive approximation. The first approach views the data as a realization of a linear, stochastic process, whereas, the second approach considers the data points as the result of a deterministic process, supposedly nonlinear. The comparison of the predictive skills of the two techniques is a strong test to distinguish between low-dimensional chaos and random dynamics. The latter methodology was extended more by the use of Higuchi (1988, 1990) methodology, in order to extract maximum, quantitative information, about the time dynamics from these geoelectical signals (Cuomo et al. 1999). Cuomo et al. (2000) used a slightly different statistical methodology in order to discriminate extreme events in geoelectric, precursory signals with implications on earthquake prediction.

Telesca et al. (2004) applied the Principal Component Analysis (PCA) method on geoelectrical signals, measured, in the seismically active area of Basilicata region, southern Italy. The analysis showed earthquake precursory patterns in the daily variation of the principal components.

Fisher information analysis was used by Telesca et al. (2005), in order to study the time fluctuations in the dynamics of the geoelectrical data, recorded in Tito site, which is located in a seismic area of southern Italy.

Ida and Hayakawa (2006) used fractal analysis for the ULF data, recorded, during Guam earthquake in 1993, to study prefracture criticality.

Hayakawa and Timashev (2006) applied flicker noise spectroscopy in an attempt to identify precursors in the ULF geomagnetic data.

Varotsos (2005), after using statistical physics, suggests "all SES signals and activities exhibit critical behavior, while artificial noise does not". On the basis of criteria, of this kind, seismic electric signals **(SES)** are able to be discriminated from artificial noise. However, "artificial noise may some times be associated with criticality (when a system approaches a failure)" and therefore, cannot be discriminated from the SES.

In conclusion, to date a large number of methodologies, aiming to discriminate the electric, precursory signals, has been presented in seismological literature. Each one of them was applied on specific data set and seismogenic area.

Therefore, by taking into account the physical complexity of the seismic generating mechanism, it is questionable if these methodologies can be applied in a different seismogenic area and for a different precursory, electric data set, with the same successful results. The obvious question to arise is: what is the solution to this problem? In practice, there must be a universal methodology, which will be applicable to all electrical, precursory data sets. Although the answer will appear to be bizarre, it is as follows: **all anomalous, electrical signals, no matter their origin, are initially (as a working hypothesis), considered of being as seismic, precursory signals.**

In such a case, these signals have to follow simple physical laws of electric fields; such as the electrical field intensity vector should be pointing towards the current source location. This will be presented in detail in the section **(4.2.7)** to follow.

4.2.7. Basic principles of current flow in the ground.

In section **(2.5.3)** the homogeneous ground model was postulated and the resulted, equipotential surfaces in the ground, as well as the equipotential contours, formed, on the ground surface, are presented in figures **(2.5.3.1)** and **(2.5.3.2)** respectively. It must be stressed out that this model is a theoretical one and does not show any resemblance to the real, geological – tectonic conditions, which are valid for a specific location, where a monitoring site of the Earth's electrical field has been located. Therefore, it is interesting to study the way the current flows in the ground and the way its flow is modified, due to usual geological – tectonic features, met, along its path.

A simple, common, geological complex is the stratigraphic one. That is the ground underneath the surface consists of different, horizontal, geological formations of various thickness and depth extent. This is illustrated in the following figure **(4.2.7.1).** The thickness of each layer is denoted by the symbol (h_i) for the i_{th} layer, the resistivity of each geological formation is represented by the symbol (ρ_i) for the i_{th} layer and the symbol (H_i) represents the depth of each geological interface from the ground surface. The deepest formation is supposed to extend to infinity.

Let us assume that, exists a horizontal total current flow (I_0), due to a distant current source. Each geological layer is penetrated by a fraction of the total current, the magnitude of which fraction is controlled by the resistivity of each formation. The total potential, developed, on a point on ground surface, due to all geological layers, is represented as:

$$U_x = f(h_1,..h_n, \rho_1,...\rho_n, x, I_0) \qquad (4.2.7.1)$$

Where: **x** is the distance of the surface point where the potential is measured from the current source and $\mathbf{I_0}$ is the total current flow.

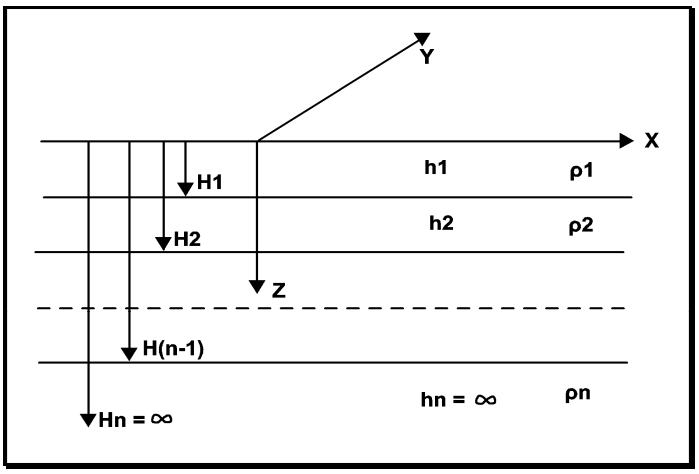

Fig. 4.2.7.1. Sketch presentation of a horizontally, stratified, multi-layer Earth (after Bhattacharya and Patra, 1968).

A detailed presentation of equation **(4.2.7.1)** was given by Grant and West (1965), Kunetz (1966), Bhattacharya and Patra (1968) which was based on the original work of Stefanescu and Schlumberger (1930) and can be found in many other Applied, Geophysical textbooks which refer to the electrical methods, too.

An immediate result of equation **(4.2.7.1)** is that, by using very long dipoles for the measurement of the Earth's potential, this potential is influenced drastically by the local, stratigraphic conditions of the place where the dipoles are installed. Consequently, the **dV/dL = constant** criterion, used by the **VAN** group (Varotsos and Alexopoulos, 1984; Varotsos and Lazaridou, 1991) cannot be used, unless both dipoles, short and long are appreciably shorter than the wavelength of the shortest lateral - stratigraphic – tectonic discontinuity which is present, at the regional place of installation.

Taking into account the intense tectonics – lateral discontinuities and stratigraphy of Greece, the use of long dipoles should be avoided, whenever it is possible. A typical "wrong" case of an installation is the one of Pirgos monitoring site (Varotsos et al. 2006). There are used long dipoles of the order of 11Km, while one electrode (in Pirgos) is installed in upper terrace (conglomerates) formations, and the others are located on the outcrops of the limestone basement of a wider deep tectonic sink. Moreover, the different stratigraphy and the present tectonics at each monitoring site affect the "apparent" resistivity **(ρ),** which is used in the calculations of the current density **(J)**.

The effect of the stratigraphy and the tectonics on the potential which develops on ground surface will be demonstrated in a different way by the following analysis of a current that flows through a geological interface. It is assumed that, a current of density **J1** crosses the boundary of two geological formations of resistivities ρ_1 and ρ_2**.** This is shown in the following figure **(4.2.7.2).**

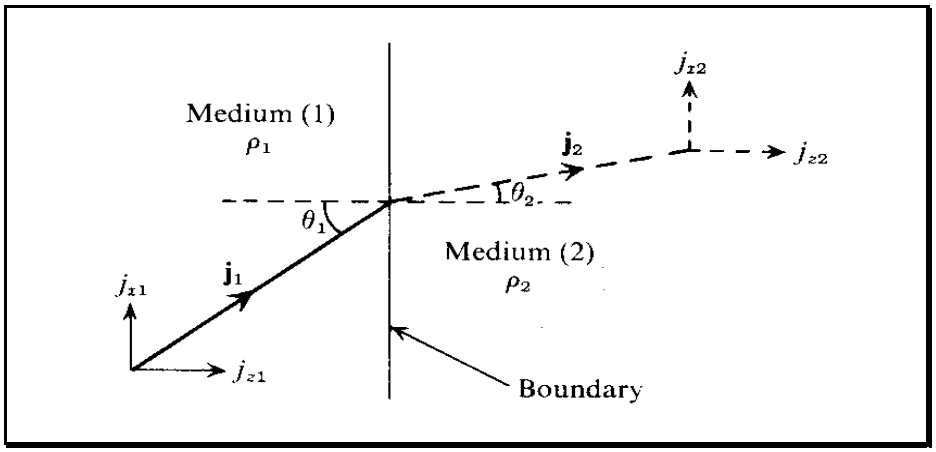

Fig. 4.2.7.2. Current of density J_1 crosses the medium boundary at angle θ_1 and enters medium (2) with a current density J_2 at an angle θ_2 (after Telford et al. 1976).

Using Ohm's law, in terms of current density, it is obtained:

$$J_{x1}\rho_1 = J_{x2}\,\rho_2 \quad \text{and} \quad j_{z1} = j_{z2} \qquad (4.2.7.2)$$

Dividing these expressions, we have:

$$\rho_1\,(J_{x1}/\,j_{z1}) \;=\; \rho_2\,(J_{x2}/j_{z2}) \quad \text{or} \quad \rho_1\tan\theta_1 \;=\; \rho_2\tan\theta_2 \qquad (4.2.7.3)$$

so that :

$$\tan\theta_2 \,/\, \tan\theta_1 \;=\; \rho_1 \,/\, \rho_2 \qquad (4.2.7.4)$$

Thus, the current lines are bent in crossing the boundary. If $\rho_1 < \rho_2$**,** they bent towards the normal and vise versa.

As a result of the previous analysis, the potential distribution, due to horizontal, geological boundary, is modified accordingly. This effect is shown in the following figure **(4.2.7.3).**

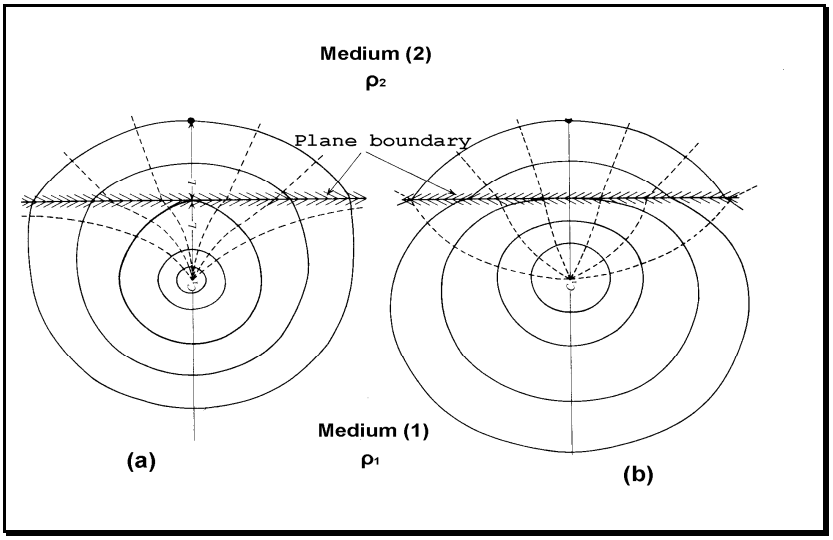

Fig. 4.2.7.3. The equipotential lines of an electric field are distorted, due to the presence of a boundary, between two geological formations, of different resistivity (after Telford et al. 1976). Solid lines represent the equipotential lines, while dashed lines represent the current flow.

The latter is visualized on surface potential contours as “shrinking” or “expanding” of them, as it is shown in the following figure **(4.2.7.4).**

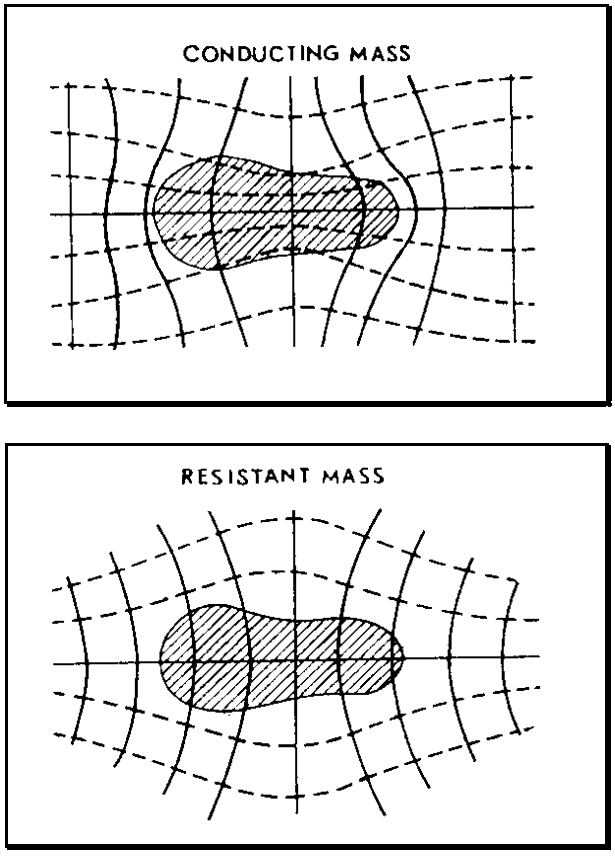

Fig. 4.2.7.4. Distortion of surface potential contours, due to the presence of conducting or resistant subsurface 3-D structure (after Kunetz, 1966)

In practice, care must be taken when a monitoring installation, for the Earth's electric field registration, is to be located at a certain place, so that the electric dipoles are definitely shorter than the dimensions of the subsurface conducting or resistant mass and are located over its center, where the distortion is less in terms of change in azimuthal direction of current flow.

A completely different approach is followed, when the maximum of signal, is the target. This is demonstrated in the following figure **(4.2.7.5).**

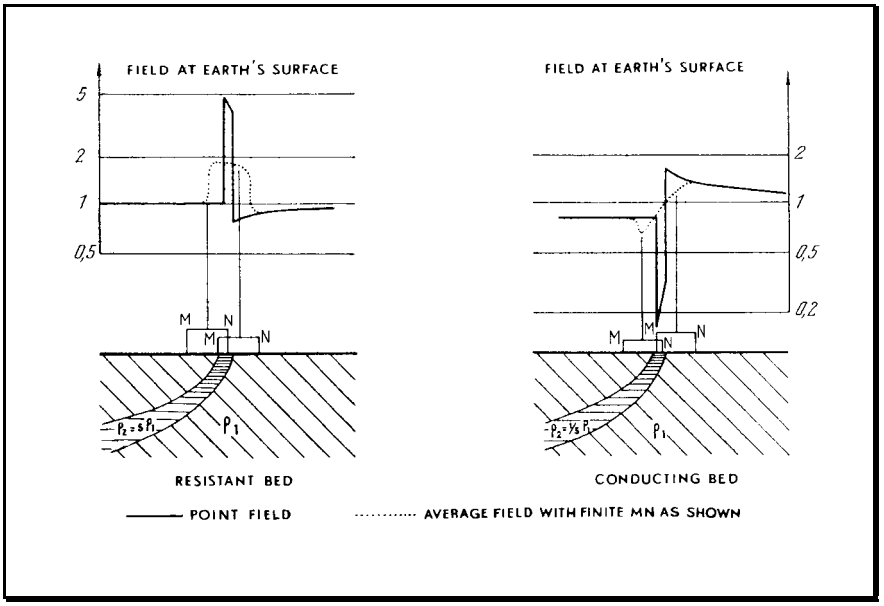

Fig. 4.2.7.5. Distortion of the Earth's potential field, due to the presence of a resistant bed (left) and a conducting (right) one (after Kunetz, 1966).

The latter demonstrates the practice, followed by the **VAN** team, to locate one electrode of the receiving dipole on a discontinuity (edge of a dyke), in order to achieve large amplitudes of the recorded SES.

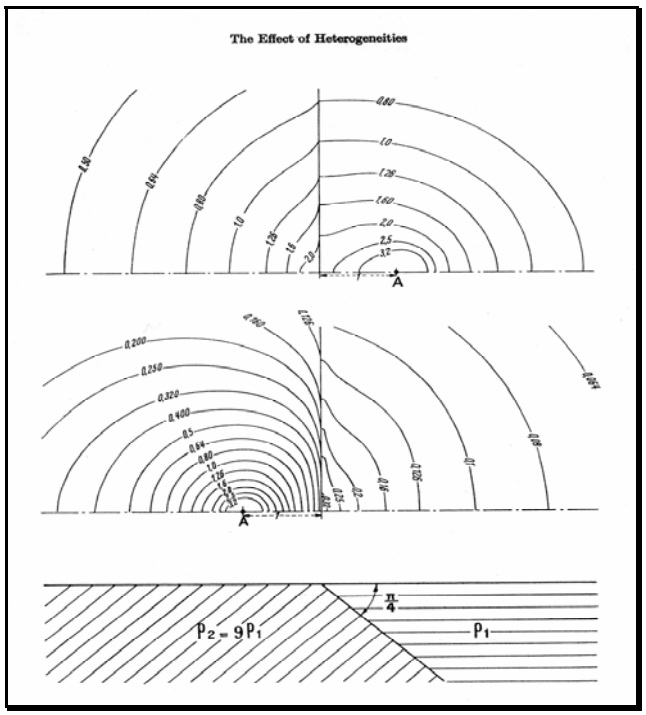

Fig. 4.2.7.6. Distortion of the Earth's potential field observed, due to the presence of an inclined, lateral discontinuity (lateral geological contact) between two different geological formations (Kunetz, 1966).

Another cause which distorts the Earth's electric field is the presence of intense topographic relief. Actually, the horizontal gradient of the field changes drastically, in the vicinity of "hills" and "depressions" of the ground surface. This is demonstrated in the following figure **(4.2.7.7).**

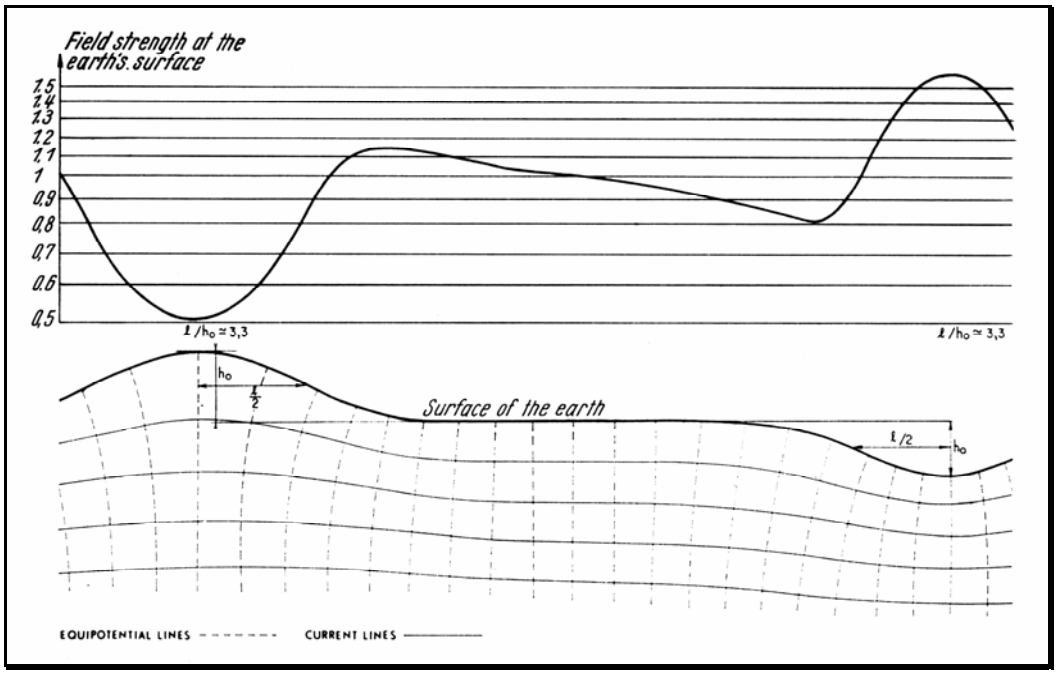

Fig. 4.2.7.7. Distortion of the Earth's potential field is demonstrated, due to the presence of intense topographic relief (after Kunetz, 1966).

Evidently, all the aforementioned causes distort the amplitude of the Earth's electrical field and therefore, the prerequisite of having registrations which correspond to a "unit trigonometric circle" compliant registration system is not fulfilled. The result is that, generally, in such a case, it is not possible to perform azimuthal determination of the Earth's electric field intensity vector. Additionally, it is not possible to correlate electrical field intensity vectors, calculated by different monitoring sites, since these reflect the local stratigraphic and tectonic conditions, met, at each station, while using them for epicenter location (Varotsos and Alexopoulos, 1984), is consequently, rather unjustified. This explains the reason, why Varotsos (2005) made the following statement for the epicentral area determination "A unique epicentral prediction still seems difficult"

The latter presentation dictates the place a monitoring site of the Earth's electric field should be located.

a. Site selection in a flat area. Preferable is the center of a sedimentary basin or an area with very small topographic relief.
b. The electrodes should be located in, as close as it can be, similar geological conditions far from surface tectonic features (basement outcrops etc).
c. The length of dipoles should be kept within the range extent of homogeneous ground.

What must be kept in mind is that, the intensity vector of the Earth's electric field, measured, at a specific place, changes in scalar value, due to different local, electrical resistivity stratigraphic conditions in the ground. On the other hand, this has, as an effect, the inability to correlate the scalar values of the electric field intensity vectors, of different monitoring sites, aiming into epicentral area determination. As long as it has not been distorted from the previous causes, it maintains its azimuthal direction properties, due to the electrical mechanism which generates it, in other words it points towards the current source location.